Astronomy & Astrophysics

(CAUCASUS)

International Scientific Journal

5

SAMTSKHE-JAVAKHETI STATE UNIVERSITY PRESS

Astronomy & Astrophysics

(CAUCASUS)

Samtskhe-Javakheti State University Press

Email: astronomy@sjuni.edu.ge

Astronomy & Astrophysics (Caucasus) 5, (2020) (3-6)

ON A NON-THERMAL VELOCITIES IN THE SOLAR CORONA

ALIYEVA Z.F.
Department of Astrophysics, Baku State University, Z. Khalilov str.23, AZ 1148, Baku, Azerbaijan
e-mail: zaminaaliyeva@bsu.edu.az

Abstract. The paper considers the change in the width of the coronal spectral lines along the solar disk. The change in the width of the coronal lines along the solar disk is sometimes contradictory. Often, the widths of the lines are changed little along the solar disk. We explain such cases by joint motion on slow magneto-sound and Alfven waves.

It is shown that the relation between the motion velocities on the Alfven wave δv and the phase velocity v_a is $\delta v \sim v_a$ meaning that with an increasing (decreasing) phase velocity δv, the motions increase (decrease). Since with the height above the limb, the phase velocity of the Alfven waves are increased due to the decreased density, the phase velocity is increased, therefore the motions velocities are increased as well. This explains the increasing widths of lines above the limb.

Keywords: Solar corona, MHD waves, non-thermal velocities.

1. Introduction

According to the studies of many authors, the width of the coronal lines above the solar disk is almost unchanged. The width of the coronal lines is determined by two motions: thermal motions of ions and non-thermal motions caused by slow magneto-acoustic waves propagating in the corona and mostly by Alfven waves and turbulent motions [5, 7, 11, 10, 1 and references of these works].

Turbulent motions broaden the spectral lines most likely the equally across the solar disk. If non-thermal motions in the corona were caused only by turbulent motions and motions on Alfven waves, then the values of non-thermal velocities would increase from the center of the disc to the limb. But, as we will see below, in many cases, there is an isotropy of non-thermal velocities along the solar disk.

We assume that the isotropy of non-thermal movements is caused by the motions on slow magneto-sound waves and on Alfven waves. In the given paper, we consider the isotropic case of broadening of the coronal lines of MHD waves, without involving turbulent motions.

Note that since at all coronal points a given coronal line is radiated at the same temperature, we must say that the changes in the width of the coronal line are caused by non-thermal motions on MHD waves.

The given paper considers the possible role of MHD waves in the isotropic broadening of coronal lines, as well as the change of velocities on Alfven waves with height.

2. Isotropy of the widths of the coronal lines along the Solar disk

During the observations, the authors obtain a spectrum from a large disk area (1″·120″, for example, see [4]). Clearly, there are numerous Alfven and slow magneto-sound waves in this area. Therefore, the observed coronal spectral line broadens simultaneously by motions on both Alfven and slow magneto-sound waves.

In other words, the non-thermal velocity found on the Doppler width of the line is the square of the sum of the squares of the most probable velocities of the motions on Alfven and slow magneto-sound waves:

$$V_{nt}^2 = \upsilon_{nt}^2(s) + \upsilon_{nt}^2(a). \quad (1)$$

Here: $\upsilon_{nt}(a)$ and $\upsilon_{nt}(s)$ nt (s) are non-thermal velocities of Alfven and slow magneto-sound waves,

respectively.

The question is how to find the values of $\upsilon_{nt}(a)$ and $\upsilon_{nt}(s)$. We will calculate the values of these quantities based on the following consideration, bearing in mind that the waves in question propagate in magnetic tubes that are perpendicular to the surface of the Sun.

Further, the motions of the slow magneto-sound waves occur along the magnetic tube, and the motions on the Alfven wave occur perpendicularly to the magnetic tube.Then, during the observations in the center of the Solar disk, the line of sight is perpendicular to the motions on the Alfven wave and therefore in the center of the disk $\upsilon_{nt}(a)=0$, while the value of $\upsilon_{nt}(s)$ is maximum; near the limb, on the contrary: $\upsilon_{nt}(a)$ is maximum, and $\upsilon_{nt}(s)=0$. Obviously, the non-thermal velocities observed on the centre of the disk are the velocities of motions on slow magneto-sound waves, and the non-thermal velocities observed closer to the limb are the velocities of motions on the Alfven wave. As an example, we can show coronal line λ1037 OVI from Table 1 [5]: in the centre of the solar disk, the value of non-thermal velocities is υ_{nt}=32km/s, and closer to the limb υ_{nt}=34km/s.

Thus:

$$\upsilon_{nt}(s)= 32 \text{ km / s}, \upsilon_{nt}(a)=34 \text{ km / s}.$$

Obviously, depending on angle θ on the surface of the Sun, the total velocity will change as follows:

$$V_{nt}^2(\theta)= (32 \cos\theta)^2 +(34 \sin\theta)^2 \quad (2)$$

The values of $V_{nt}(\theta)$ are calculated for values θ=0, 10, 20,….90° .

θ, (°)	0	10	20	30	40	50	60	70	80	90
V_{nt}, (km/s)	32,00	32,06	32,23	32,51	32,85	33,18	33,51	33,78	33,94	34,00

As it can be seen from the table above, in this example, the values of non-thermal velocities are almost constant throughout the Sun disk.

In [7], coronal lines MgX 609 and Mg X 625 were observed near the limb on the disk and above the limb. A portion of r/R was observed in the interval 0.7-1 on the disc. The values of non-thermal velocities, determined by the observed Doppler widths of the indicated lines in the indicated interval turned out υ_{nt}=26 km/sec. Besides, it turned out that this value is constant in the whole indicated interval.

The authors believe that the observed non-thermal velocities are motions on the Alfven wave.

In this case, expression (1) takes the form:

$$V_{nt}(\theta) =\upsilon_{nt}(\theta)= 26\sin\theta \quad (3)$$

In the given paper, the values of non-thermal velocities are given for the following values sinθ= 0.7, 0.8, 0.9, 1.0.

Using expression (3), we find:$V_{nt}(45^\circ)$=18.2; $V_{nt}(54^\circ)$=21.8; $V_{nt}(65^\circ)$=23.4; $V_{nt}(90^\circ)$=26 km/sec.As it can be seen, if non-thermal velocities were the velocities of motions only on the Alfven wave, the values of these velocities would decrease toward the centre of the disk.

Now, let us consider the assumption that thermal motions are created by both Alfven waves and slow magneto-sound waves. Obviously, in the center of the disk, the velocity of motions on Alfven waves is equal to zero, since these motions are perpendicular to the line of sight. The authors believe that the values of non-thermal motions are uniform throughout the disk. In this case, these motions should satisfy expression (1). This means that in the center of the disk $\upsilon_{nt}(s)$=26 km/sec. The observed value of non-thermal velocities on the limb is the velocities of motions on Alfven waves. So, according to expression (1) for a given case, we can write down:

$$V_{nt}^2(\theta)=(26\cos\theta)^2 +(26\sin\theta)^2=26^2.$$

Hence: $V_{nt}(\theta)$=26 km/sec. In other words, if non-thermal velocities are “created” by the combined action of slow magneto-sound and Alfven waves, then non-thermal velocities will be uniform throughout the

disk. Therefore, we can conclude that the observed isotropic distribution of non-thermal velocities on the Sun disk is explained simultaneously by motions on Alfven and slow magneto-sound waves.

The determination of non-thermal velocities on the lines λ195,12 FeXII and λ 202,94 FeII showed [11] that the values of these velocities from the center of the disk to the limb are constant and equal to 36 km/sec (Fig. 7). This interesting result can only be explained by the fact that these velocities are the motions on Alfven and magneto-sound waves, and the amplitude of the velocities of the motions on both waves is the same. We emphasize that the authors explain this fact that the source of non-thermal motions are turbulent motions in the corona. The observed values of non-thermal velocities in line λ624.94 MgX are almost constant on all disk of the Sun ([10] Fig. 6).

According to observations [9], the widths of the line λ625 MgX on the disk closer to the limb significantly differ with various data and have a somewhat complex appearance with a tendency to grow to the limb. Unfortunately, the authors do not explain this observational fact.

Based on the observations of some spectral lines arising in the upper atmosphere and in the corona, the authors concluded that non-thermal velocities change slightly along the solar disk, i.e. they are isotropic.

According to the observations [8], the width of line Fe X 6374 (red line) above the solar limb increases with height, while the width of line FeXIV 5303 (green line) decreases.

The authors (et al., see references in the present work) explain this by the fact that, according to the line of sight, there are many undisturbed structural elements with different temperatures in the corona. As a result, the velocity of the Alfven wave decreases and therefore the width of the blue line decreases with height. But we must indicate that the velocity of the Alfven wave is independent from temperature. Most likely, unresolved structures with different densities are found along the line of sight.

3. On change in non-thermal velocities over the solar limb

The results of determining changes of the non-thermal velocities value with a height above the limb are very contradictory.

In [2], the results of measurement of the values of non-thermal velocities in the corona, depending on the height above the limb, are shown from observations in the line λ 5303 Fe XIV at the coronagraph of the Sacramento Peak Observatory. Figure 8 shows that the values of non-thermal velocities decrease with increasing height.

According to the observations on the SUMER / SOHO spectrograph in ultraviolet lines, the authors of [3] found that the velocities of non-thermal motions increase with height (Fig. 4).

It is of interest to look at the theoretical dependence of the velocities of motions on the Alfven wave (which lead to the broadening of the coronal emission lines observed on the limb) with the phase propagation velocity of this wave and compare it with the observations. Mean square value of the velocities on the Alfven wave is proportional to $\rho^{-1/4}$ [4]:

$$(\delta v^2)^{1/2} \sim \rho^{-1/4}$$

The phase velocity of the Alfven wave is proportional $\rho^{-1/2}$:

$$v_a \sim \rho^{-1/2}$$

Consequently:

$$\delta v \sim v_a^{1/2} \quad (4)$$

Since the density decreases with the height in the corona, the velocities at the Alfven wave should increase with the height. The comparison between the calculated values of non-thermal velocities on the Alfven wave and the observed values along the SiVIII line 1445.75 made by the authors shows a good agreement between these values: both velocities (the calculated and the observed) increase with the height (Fig. 4). This suggests that the observed non-thermal motions are motions on Alfven waves. The phase velocity of the Alfven wave increases with the height in the corona due to a decrease in density.

Expression (4) shows that with the height in the corona, the amplitude of the velocities of motions on the Alfven wave increases as well.

The conflicting results of measuring the width of the lines in the height above the limb remains unexplained so far. If the widths of the coronal lines were expanded only by motions on Alfven waves, then they would show the growth with height above the limb. The contradictory results of the measurement of the widths of the lines in height above the limb remain unexplained.

Thus, we conclude that if non-terminal motions are motions on Alfven waves, the non-terminal motions must grow with the height on the limb.

4. Conclusion

The study of changes of coronal lines along the solar disk is of interest from the point of view of revealing the mechanism used by non-thermal motions to create broadening spectral lines. The broadening of coronal lines is caused by MHD waves: slow magneto-sound and Alfven waves, as well as turbulent motions. The observational data are contradictory, but mostly, the widths of the spectral lines are almost constant across the solar disk. In the present paper, we investigate the cases of almost constant (isotropic) line widths over the solar disk. We conclude that in this case, the motions on slow magneto-acoustic and Alfven waves can be the mechanisms for broadening coronal lines without involving turbulent motions.

We find that there is a relation $\delta v \sim v_a$ between the phase velocity of the Alfven wave and the motion velocities on this wave, showing that with increasing (decreasing) of the phase velocity of the Alfven wave, the motions velocities increase (decrease) on that wave. This effect can explain the increasing of the line widths over the solar limb. This effect can explain the increase in line widths above the solar limb.

References

1. Chae J., Shuhle U. and Lemaiere Ph.: SUMER measurements of non-thermal motions: constraints on coronal heating mechanisms . ApJ, v. 505, p. 957- 973, 1998
2. Contesse L., Koutchmy S., and Viladrich C.: Analysis of non-thermal velocities in the solar corona. Annales Geophysicae (2004) 22: 3055–3062.
3. Dolla L. and Solomon J.: Solar off-limb line widths with SUMER: revised value of the non-thermal velocity and new results Ann. Geophys. 27, 3551–3558, 2009.
4. Doyle J.G., Banerjee D. and Perez M.E.: Coronal line –width variations. Sol. Ph, v. 181, p. 91-101, 1998.
5. Erd´elyi1 R., Doyle J.G., Perez M.E., and Wilhelm K.: Center-to-limb line width measurements of solar chromosphere, transition region and coronal lines. A&A, v.337, p.287- 293. 1998.
6. Hasegawa A. and Uberoi Ch.: The Alfven waves. United States Department of Energy. 1982, p.3.
7. Hassler D. M., Rottman G. J. Shoub E. C. and Holzer T.E. : Line broadening of Mg X λλ 609 and 625 Coronal emission lines observed above the Solar limb. ApJ, v. 348, p. L77-L80. 1990
8. Krishna Prasad S., Jagdev Singh and Banerjee D.: Variation of Emission Line Width in Mid- and High-Latitude Corona- arXiv:1210. 6434 v1 [astroph.], 2012.
9. O'Shea E., Banerjee D., and Poedts S.:Variation of coronal line widths on and off the disk. A&A 400, 1065–1070 (2003)
10. Stucki K., Solanki S. K., Pike C. D., Schuhle U., Ruedi I., A. Pauluhn1; 6;7, and A. Brkovi: Properties of ultraviolet lines observed with the Coronal Diagnostic Spectrometer (CDS/SOHO) in coronal holes and the quiet Sun. A&A, A&A 381, 65-667 , 2002.
11. Ying Li and Ming-De Ding: Measurements of a spectral lines observed with Hinodes/EIS as implications for Coronal heating. Research in Astron. and Astrophys, v. 9, p. 829-840, 2009.

Astronomy & Astrophysics (Caucasus) 5, (2020) (7-36)

CATALOG KVARATSKHELIA-SAARI-SHORTHILL

O. I. KVARATSKHELIA

E. Kharadze National Astrophysical Observatory

Email: kvara_otar@mail.ru

Abstract

The studies accomplished at the end of the past century, comparing various optical characteristics of lunar soils and their terrestrial analogs, showed that it is possible to identify different degrees of packing of the lunar surface matter by remote sensing methods. The normal albedo ρ0 and the maximum degree of polarization Pm are used as the initial characteristics of the reflectivity of a finely dispersed substance.
Key words: Moon, Polarization, Albedo

It was found that on a two-dimensional histogram of the ρ0 (Pm) type, among the points of measured albedo values and the maximum degree of polarization of a number of finely dispersed terrestrial magmatic samples of a known grain-size and mineralogical composition, two types of sequences can be distinguished. One family of functions characterizes changes in ρ0 and Pm of a substance of the same type with insignificant variation in chemical composition. Another is a change in the optical characteristics of rocks with similar particle diameters, with a change in the mineralogical and chemical composition [1]. Test studies were carried out in the area of volcanic deposits in Kamchatka, based on polarized aerial photography [2].

The results of numerous studies of analogs of lunar soil made it possible to introduce the concept of an optical parameter of the relative porosity of a reflecting substance of the following form: $\Delta\Psi = il g\rho + klgP$m, which quantitatively describes the ability of the uppermost soil layer to absorb and scatter sunlight [3].

This parameter (in a simplified form ρ0 (Pm)) is physically close to the second non-normalized Stokes parameter. An analysis of the cumulative results showed that the adopted parameter shows the real relationship between the physical and the mechanical properties of the soil in its natural bedding with the characteristics of scattered light and describes the properties of not only a reflecting optically thin layer of matter, but also deeper underlying layers. The technique makes it possible to identify large-scale irregularities in the density of the material using synthesized images.

A number of studies in this direction make it clear that it is possible to assess the effective size of particles of a finely dispersed material in the surface layer [4]. As a result of laboratory measurements, the ratio between the normal albedo, the maximum degree of polarization and the average particle size was obtained: lgΔΨ=4,8lgρ0+ 3,4lgpm-7,1.

Identification of areas with a predominant distribution of the fine fraction in the surface layer of the Moon is extremely important at the early stages of design work on the lunar base, since it is in the mass of the fine fraction that the largest amount of hydrogen and helium-3, the main elements of the natural resources of the Moon, is contained. As it is known from the works by various authors, over 80% of hydrogen and helium-3 in the samples of lunar rocks delivered to the Earth was found in a fine fraction with a particle size of up to 45 microns. From this point of view, according to our data [1], the south of the Sea of Abundance is promising.

One of the most important practical conclusions made by B. Hapke [5] in the theoretical consideration of the phase function of the Moon was the determination of the parameter of the relative density of lunar surface H. This value characterizes the packing of particles of the uppermost extremely fragmented and porous layer of the lunar regolith. The Hapke values of this parameter are determined by the following

formula $H=K\sqrt[3]{(d/d_0)^2}$ .Here d0 is the density of the rock, d is the density of the lunar surface rocks, the coefficient K = 2 for the lunar sites. Measurements of parameter H over the lunar disk for small areas (∼10") revealed significant differences in H from place to place within 0.1 <H <1.1 [6], with an average value of the relative density parameter for the visible hemisphere of the Moon equal to 0.5. Mapping of this parameter directly using the formulas of the Hapke photometric function is possible only by points. At the same time, it would be very useful to know the prevalence of this parameter over the lunar disk to reveal the presence of large-scale non-homogeneities in the relative density of the lunar surface.
We set the task to reveal the relationship between the Hapke parameter - H and the optical parameter of relative porosity. For this purpose, on the 40-cm Zeiss refractor of the Abastumani Astrophysical Observatory (F = 6.8m) at a wavelength ƛ = 0.440 μm, with a working aperture d = 7 ". 5, at close phases for both quarters of the moon, in quadratures, when the degree polarization reaches its maximum value (phase angle α∼ ±900), O. Kvaratskhelia accomplished polarimetric observations of all points of the Saari-Shorthill catalog [6], for which the normal albedo was measured with high accuracy.
The observations were accomplished using an automatic electro-polarimeter of the Abastumani Astrophysical Observatory [7]. The results of these observations for 190 points of the catalog [6] (77 points for the first quarter and 113 for the last one) were published in article [8] as KVARATSKHELIA-SAARI-SHORTHILL catalog. Additional polarimetric observations of objects from the Saari-Shorthill catalog with the same equipment were accomplished in 2005-2009 [9, 10, 11].

This article presents the results for about 300 catalog points [7]. At the end of the article, we present the complete KVARATSKHELIA-SAARI-SHORTKHILL catalog with the following designations: ƛ, β-selenographic coordinates of the observed areas; HX100 is the Hapke parameter and ρ0% is the normal albedo of the sites according to the catalog [6]; Pm% is the results of polarimetric observations by O. Kvaratskhelia; ρ0 (Pm)is the parameter corresponding to the second unnormalized Stokes parameter in a physical sense and being proportional to ΔΨ; the index is the qualitative characteristics of the lunar regions according to the catalog [6]. For example: A designates area with medium albedo, B means bright, D means dark, C is the craters, etc. α is the angle of the moon phase during the observations. At the end of the work, Moon maps are given, which are taken from the Saari-Shorthill catalog [6] with the designations of the measured lunar areas, Fig. 4a - 12a, for the western hemisphere of the Moon and Fig. 4b - 12b, for the eastern hemisphere of the moon.
The observation results are as follows:
1. Based on our subsequent observations to the photo-polarimetric catalog of Kvaratskhelia-Saari-Shorthill [8], the polarization data have been added. Now, the catalog for 284 lunar surface objects consists of the following data: normal albedo, Hapke parameter and degree of polarization.
2. We compared the values of the Hapke parameter and the product ρ0 (Pm) at each observation point [8], and did not reveal a direct relationship between them. Then we compared the average values of ρ0 (Pm), at the intervals of changes in the parameter H: 0.1-0.2, 0.2-0.3, etc. [8]. In this case, a clear direct dependence of changes in ρ0 (Pm) and the Hapke parameter was revealed, and it is individual for each quarter. This result needs to be verified, since it is necessary to explain why the average values of parameter ρ0 (Pm) for the sections in the first quarter are 10% higher than for the last, at the same values of phase angles ∼ ±900. It can be assumed that, on average, the lunar regolith in the last quarter is represented by a more finely dispersed matter. It was here where late marine volcanism developed, and the surface soil can be enriched to date with microscopic ash particles smoothing the Pm polarization values. But perhaps, the answer must be sought in the difference between the mineralogical composition of the western and the eastern parts of the lunar disk. However, the identified correlation of these parameters makes it possible to calibrate the images synthesized as a function of the optical parameter of relative porosity ΔΨ of the lunar regolith in units of the H parameter proposed by Hapke.

Conclusion

In the given paper, data on the degree of maximum polarization are added to the Saari-Shorthill photometric catalog. The dependence of the second non-normalized Stokes parameter and the Hapke parameter is studied and a clear trend was identified that proves the relationship between them.

References

1.Kvaratskhelia O.I., Novikov V.V., Busarev V.V. Maturity factor of lunar regolith according to polarimetric observations // Proceedings of the Abastum Astrophysical Observatory. 1989. T. 68.pp.111-123.

2. Novikov V.V., Porosity of deposits of terrestrial and lunar basalts according to data on their albedo and degree of polarization // Complex research of the Moon. M.: Publishing house of Moscow State University, 1986, pp. 108-122.

3. Novikov V.V., Goryachev M.V. On the mechanism of interrelation of physical, mineralogical and optical properties of finely dispersed soils // Proceedings of GAI Sh. 1984. Vol. 56. pp. 113-125.

4.Dollfus A., Deschamps M. Grain size determination at the surface of Mars. Lunar and planet//Science.Houston,1985.V.16.pp. 193-199.

5.Hapke B., Optical properties of the lunar surface // Physics and astronomy of the Moon. Moscow: Nauka, 1973.pp. 166-229.

6.Saari J.M., Shorthill R.W. Photometric properties of selected lunar features .NASA. 1969.CR-29.187p.

7. Kvaratskhelia O.I, Spectropolarimetry of the lunar surface and lunar soil samples. Bull. Abastumani.astrophiz. observatory Gruz.An. 1988. No. 64. p. 312.

8. Kvaratskhelia O.I, Novikov V.V. Optical parameter of the relative porosity of the lunar regolith from polarimetric observations. Astron. Bulletin 1992. Vol.26. No. 6. pp. 3-13.

9. Kvaratskhelia O.I, International Scientific Konference ‘’Problems of Modern Astrofysics’’report “Spectropolarimetry of the Moon’’. Akhaltsikhe. 2015.

10. Kvaratskhelia O.I, Ivanidze R.,Gigolashvili Sh. Spectropolarimetry of the Lunar Surface and Ground Samples. Astronomy and Astrophysics(Caucasus)1, 2016, pp.49-52.

11. Kvaratskhelia O.I, Chigladze R., et.al. Multiparameter Atlas of the Moon. E.Kharadze Abastumani Astrophisical Odservatory.pp.1-180, 2019.

CATALOG KVARATSKHELIA-SAARI-SHORTHILL

N	λ^0	β^0	Hx100	ρ_0%	Pm% 440nm	ρ_0xPm	α^0	INDEX	Figure N
1	2	3	4	5	6	7	8	9	10
				First Quarter					
1	9,40	18,05	92,90	7,04	14,30	100,7	87,30	D16	4b
2	19,92	16,90	59,75	6,40	19,31	123,6	99,60	D17	4b
3	23,27	24,22	45,31	6,26	19,20	120,2	99,70	D18	4b
4	28,12	24,20	47,95	6,21	19,54	121,3	99,60	D19	4b
5	36,37	14,92	64,33	6,31	19,17	121,0	99,50	D20	4b
6	39,32	5,87	56,72	6,36	17,36	110,4	99,50	D21	4b
7	43,67	5,85	68,88	7,21	18,61	134,2	99,50	D22	4b
8	46,27	-0,05	51,97	6,68	16,53	110,4	99,50	D23	4b
9	51,33	-5,97	53,48	6,47	19,62	126,9	99,40	D24	4b
10	55,03	-4,23	59,46	6,94	12,60	87,4	99,40	D25	4b
11	59,35	-0,15	44,73	7,54	10,90	82,2	99,40	D26	4b
12	57,18	13,58	53,73	6,71	15,81	106,1	99,30	D27	4b
13	58,23	16,10	46,03	6,60	15,63	103,2	99,30	D28	4b
14	63,45	17,17	48,90	6,31	16,04	101,2	99,30	D29	4b
15	59,83	17,17	46,38	6,82	9,62	65,6	99,20	D30	4b
16	63,30	11,65	54,89	7,84	11,33	88,8	99,20	D31	4b
17	9,50	7,00			12,71		87,30	A16	5b
18	10,48	44,42	37,54	10,11	9,33	94,3	87,30	A15	5b
19	23,28	46,72	35,89	10,70	9,62	102,9	87,30	A17	5b
20	14,50	5,73	109,56	10,11	9,66	97,7	87,30	A18	5b
21	31,67	41,68	50,29	10,20	10,21	104,5	99,20	A19	5b
22	23,57	-1,82	104,33	9,98	9,33	93,1	99,00	A20	5b
23	37,15	-23,52	51,17	12,00	8,07	96,8	99,00	A21	5b
24	34,66	-3,38	65,94	10,69	9,64	103,0	99,00	A22	5b
25	38,42	-25,47	71,16	10,24	9,94	101,8	99,00	A23	5b
26	47,07	23,58	50,10	11,16	9,83	109,7	99,20	A24	5b
27	42,22	15,85	44,99	10,53	8,84	93,1	99,40	A25	5b
28	57,40	23,95	59,43	10,98	9,07	99,6	99,10	A26	5b
29	59,28	6,65	32,76	10,68	8,88	94,8	99,10	A27	5b
30	55,37	4,70	47,75	10,99	8,64	94,5	99,10	A28	5b
31	56,00	36,00	26,27	14,59	6,51	95,0	98,90	B31	6b
32	42,50	32,50	36,16	13,50	7,87	106,2	98,90	B32	6b
33	19,00	-6,00	62,54	13,98	6,61	94,5	98,80	B52	6b
34	21,00	-12,00	50,45	13,01	7,24	94,6	98,90	B54	6b
35	11,00	-28,00	51,04	13,31	8,26	109,9	87,30	B58	6b
36	68,00	-27,67	74,40	13,03	7,33	95,5	98,80	B63	6b
37	10,50	-27,50	53,52	14,10	7.92.	111,7	87,30	B68	6b

1	2	3	4	5	6	7	8	9	10
38	45,00	-42,00	84,13	14,29	6,65	95,0	98,80	B74	6b
39	30,00	-47,17	100,02	13,12	7,06	92,6	98,80	B76	6b
40	8,00	-53,00	52,36	14,17	7,00	99,2	87,30	B79	6b
41	11,50	-52,50	54,81	14,19	7,61	108,0	87,30	B80	6b
42	3,00	13,00	46,77	6,57	16,03	105,3	87,30	M15	7b
43	18,00	26,00	55,37	6,48	15,44	100,0	98,70	M16	7b
44	27,00	-4,50	105,19	7,23	14,24	102,9	98,50	M17	7b
45	26,00	44,50	60,38	8,88	10,66	94,7	98,70	M18	7b
46	30,00	7,00	75,85	6,42	17,07	109,6	98,60	M19	7b
47	30,00	54,00	65,19	7,38	9,28	68,5	98,70	M20	7b
48	35,00	-15,00	87,36	7,39	12,67	93,6	98,50	M21	7b
49	36,00	37,50	69,17	7,26	12,64	91,8	98,70	M22	7b
50	39,00	18,50	37,63	7,18	10,20	73,2	98,60	M23	7b
51	40,83	-46,75	50,90	15,18	6,13	93,0	98,50	M24	7b
52	52,75	-20,00	61,56	7,69	10,39	74,7	98,50	M25	7b
53	52,00	-2,50	63,12	6,55	15,28	100,1	98,50	M26	7b
54	59,00	17,00	47,67	7,74	15,24	102,7	98,60	M27	7b
55	7,03	-2,62	31,35	15,73	8,07	126,9	87,10	C6	8b
56	5,18	-7,42	89,90	19,68	6,48	126,5	87,10	C7	8b
57	12,50	6,25	11,13	12,32	9,61	118,5	87,20	C8	8b
58	15,10	3,98	11,09	10,11	11,45	115,8	87,20	C9	8b
59	15,40	-0,78	66,25	15,13	7,45	112,7	87,10	C10	8b
60	3,93	40,42	43,05	9,56	11,70	111,8	87,20	C36	8b
61	69,50	12,00	46,38	9,19	7,25	66,6	98,50	C50	8b
62	13,92	-13,73	31,78	12,02	8,06	96,9	87,10	C59	8b
63	44,08	-12,00	16,29	8,98	9,53	85,6	98,40	C60	8b
64	16,50	44,25	45,55	12,11	7,81	94,6	87,20	C69	8b
65	1,47	30,67	32,18	8,77	11,75	103,0	87,20	C75	8b
66	16,00	16,25	40,51	14,18	10,46	148,3	87,20	C76	8b
67	56,00	28,00	38,11	10,91	7,81	93,0	98,50	C79	8b
68	46,42	5,58	51,56	8,21	15,60	128,1	98,40	C88	8b
69	10,20	1,83	39,69	14,10	7,20	101,5	87,10	C112	8b
70	30,83	-10,83	40,71	10,89	8,20	89,3	98,30	R21	9b
71	0,08	38,60	30,66	8,13	11,06	89,9	87,10	R22	9b
72	54,50	-10,00	65,49	7,42	9,85	73,1	98,30	R23	9b
73	8,67	0,65	42,27	12,12	8,42	102,1	87,00	V2	10b
74	20,68	-4,92	47,84	14,87	7,00	104,1	87,00	V3	10b
75	14,22	-3,02	71,26	12,96	7,20	102,4	87,00	V4	10b
76	3,08	21,47	19,62	9,37	11,55	108,2	87,00	V6	10b
77	7,67	-0,98	45,51	12,64	7,54	95,3	87,00	V10	10b
78	6,50	-1,90	37,68	11,88	8,37	99,4	87,00	V11	10b

1	2	3	4	5	6	7	8	9	10
79	7,13	-10,80	58,20	11,97	8,06	96,5	87,00	V12	10b
80	39,52	-10,50	17,87	12,21	7,05	86,1	87,30	V13	10b
81	34,42	-1,28	34,49	10,21	8,42	85,9	87,30	V14	10b
82	6,25	26,07	88,29	7,62	11,51	87,7	87,00	V17	10b
83	20,32	-21,11	35,70	11,18	7,80	86,8	87,00	V18	10b
84	19,00	-16,58	41,00	13,31	7,51	99,9	87,00	V19	10b
85	19,67	-26,25	84,02	11,88	8,17	87,1	87,00	V20	10b
86	60,67	-25,17	75,95	13,73	8,29	113,0	87,70	T1	11b
87	57,08	-19,42	93,03	13,96	12,07	168,5	87,70	T2	11b
88	51,83	-31,83	31,67	20,30	8,67	174,8	87,70	T3	11b
89	47,62	-1,83	89,68	6,88	17,90	123,1	87,90	T4	11b
90	27,75	-28,00	46,61	12,97	7,91	102,6	87,70	T5	11b
91	32,72	-0,43	90,34	14,55	9,23	134,3	87,90	T6	11b
92	29,33	22,20	106,51	7,51	18,54	139,2	88,10	T7	11b
93	13,50	38,50	39,13	11,08	12,05	133,5	88,70	T11	11b
94	9,75	21,00	57,92	5,60	20,36	116,8	88,00	T12	11b
95	4,08	-4,75	54,54	11,19	8,91	110,9	87,90	T14	11b
96	17,33	20,70	56,11	7,08	19,20	135,9	88,00	T70	11b
97	39,53	36,08	47,53	7,93	9,75		89,00	T74	11b
98	22,00	13,50	59,05	5,75	21,51	123,7	88,00	T76	11b
99	6,80	13,00	47,20	6,22	18,22	113,3	88,00	T77	11b
100	16,12	41,37	47,27	11,32	9,63	109,0	88,70	T78	11b
101	38,50	44,07	6,08	11,50	10,81		88,70	T79	11b
102	20,42	-22,58	45,80	10,95	8,01	87,7	87,80	T83	11b
103	21,40	-22,58	55,97	11,53	8,51	98,1	87,80	T84	11b
104	22,08	-22,58	50,97	11,37	8,43	98,1	87,80	T85	11b
105	8,00	24,25	44,80	6,09	19,56	119,1	88,40	T86	11b
106	10,00	24,25	50,58	6,03	19,54	117,8	88,40	T87	11b
107	12,00	24,25	54,22	5,85	19,31	113,0	88,30	T88	11b
108	14,00	24,25	60,91	6,37	18,29	116,5	88,30	T89	11b
109	16,00	24,25	49,91	6,37	18,92	120,5	88,30	T90	11b
110	18,00	24,25	70,88	6,75	20,21	136,3	88,20	T91	11b
111	20,00	24,25	47,65	6,76	18,64	126,0	88,20	T92	11b
112	24,00	24,25	58,11	6,47	18,77	121,4	88,20	T94	11b
113	26,00	24,25	49,86	6,60	19,58	129,2	88,10	T95	11b
114	28,00	24,25	47,58	6,19	18,09	112,0	88,10	T96	11b
115	29,33	24,25	47,35	6,92	18,81	130,2	88,10	T97	11b
116	3,00	26,00	62,98	7,08	13,86	98,3	89,00	T98	11b
117	4,00	26,00	45,92	9,43	14,25	134,4	89,00	T99	11b
118	6,00	26,00	16,76	7,52	10,52	79,1	88,60	T101	11b
119	7,00	26,00	35,51	7,22	14,31	103,3	88,60	T102	11b
120	8,00	26,00	30,83	6,86	19,07	130,8	88,50	T103	11b
121	9,00	26,00	65,08	6,36	19,92	126,7	88,50	T104	11b

1	2	3	4	5	6	7	8	9	10
122	21,42	9,35	60,67	5,71	21,12	120,6	87,70	S1	12b
123	24,77	2,67	100,93	6,68	19,28	128,8	87,70	S2	12b
124	23,18	1,50	73,30	6,34	87,70	119,4	87,70	S3	12b
125	42,00	-0,85	18,55	7,07	87,40	91,1	87,40	P1	13b
126	35,45	0,10	61,32	9,41	87,40	120,5	87,40	P2	13b
127	26,08	0,57	61,13	6,48	87,50	123,7	87,50	P3	13b
128	13,23	0,05	57,21	11,57	8,57	99,2	87,60	P4	13b
129	36,92	4,17	20,09	6,80	18,93	128,7	87,40	P10	13b
130	34,00	2,75	61,97	6,62	17,18	113,73	87,40	P11	13b
131	24,17	6,75	55,57	6,71	19,51	130,9	87,50	P15	13b
132	35,25	2,92	51,35	6,61	17,42	115,2	87,40	P23	13b
133	20,25	3,33	83,20	6,25	16,74	104,5	87,60	P25	13b
134	24,52	0,45	64,68	6,67	18,06	120,5	87,50	P27	13b
135	21,50	0,33	101,94	6,69	15,28	102,2	87,50	P28	13b
136	13,50	-1,50	40,92	11,82	8,53	100,8	87,60	P36	13b
137	34,00	2,67	62,30	6,60	13,84	91,3	87,40	P47	13b
138	23,62	0,75	71,24	6,43	18,47	116,4	87,50	P48	13b
					Last Quarter				
1	-62,82	17,81	25,35	5,16	11,56	75,12	87,2	D1	4a
2	-79,95	24,68	42,39	6,5	12,00	78,00	87,3	D2	4a
3	-74,07	25,72	23,18	6,82	13,82	94,3	87,40	D3	4a
4	-68,90	24,45	31,63	5,70	15,71	89,55	87,40	D4	4a
5	-61,82	6,23	24,66	5,82	14,25	82,9	87,50	D5	4a
6	-67,20	-4,00	20,88	6,96	10,22	71,13	87,60	D6	4a
7	-56,85	-5,53	27,01	5,65	16,18	91,42	87,50	D7	4a
8	54,85	32,68	30,27	6,15	12,48	76,75	87,30	D8	4a
9	-46,73	19,77	29,66	6,82	14,03	95,68	87,30	D9	4a
10	-31,15	19,68	41,04	6,89	13,58	93,57	87,20	D11	4a
11	-21,05	24,42	48,27	6,73	13,27	89,31	87,20	D12	4a
12	-9,82	24,42	58,65	6,87	14,46	94,34	87,20	D13	4a
13	-5,65	12,00	59,50	6,68	13,46	89,9	87,30	D14	4a
14	11,32	-19,57	86,34	7,05	12,69	89,5	87,60	D16	4a
15	-73,53	-0,57	21,82	11,40	6,00	68,4	87,60	A1	5a
16	-62,10	-16,30	12,48	9,97	7,15	71,29	87,80	A2	5a
17	-51,28	-20,48	27,02	10,60	7,60	80,6	87,70	A3	5a
18	-50,40	-34,12	40,32	10,86	6,47	67,03	87,70	A4	5a
19	-26,17	11,53	27,62	10,84	8,27	89,7	87,80	A5	5a
20	-28,35	50,43	46,81	10,11	7,45	88,8	87,80	A6	5a
21	-6,40	-19,82	47,60	11,25	6,57	73,90	87,70	A10	5a
22	-4,63	-17,45	75,21	10,15	7,50	76,12	87,70	A12	5a
23	-4,60	-4,77	70,79	10,31	7,10	75,47	87,70	A13	5a
24	-64,35	-10,60	26,06	10,83	6,73	12,89	87,70	A29	5a

1	2	3	4	5	6	7	8	9	10
25	-74,53	-5,73	28,17	10,50	6,50	68,2	87,80	A30	5a
26	-28,00	67,50	41,52	14,24	6,10	86,9	87,90	B34	6a
27	-67,00	-22,00	20,63	14,09	6,64	93,6	88,10	B35	6a
28	-60,00	-23,50	34,97	14,48	6,23	90,3	88,10	B36	6a
29	-2,00	-29,00	49,77	13,65	5,83	79,6	87,90	B37	6a
30	-48,50	-31,00	43,31	1391,00	6,66	92,6	88,10	B38	6a
31	-12,00	-32,00	49,88	13,50	6,66	89,9	87,90	B39	6a
32	-19,17	-39,50	62,16	1375,00	6,45	88,7	87,90	B40	6a
33	-19,83	-40,67	32,26	14,15	6,30	89,1	88,00	B41	6a
34	-20,00	-42,50	49,71	14,12	6,40	90,4	88,00	B42	6a
35	-19,83	-45,00	40,74	1388,00	6,25	86,7	88,00	B43	6a
36	18,50	-45,17	73,73	15,00	6,05	90,7	88,00	B44	6a
37	-17,00	-49,00	58,46	14,02	6,25	87,6	88,00	B45	6a
38	-17,50	52,00	35,75	14,42	6,29	90,7	88,00	B46	6a
39	-7,50	-52,67	70,28	15,19	5,26	79,9	88,00	B47	6a
40	-2,50	-58,00	26,03	14,94	5,41	80,8	88,10	B48	6a
41	-29,00	-57,17	55,91	12,19	6,30	76,8	88,10	B49	6a
42	-37,50	-58,83	65,81	11,91	6,31	75,1	88,10	B50	6a
43	-20,50	-62,33	48,40	13,71	5,72	78,8	88,10	B51	6a
44	-65,00	-5,00	10,00	6,41	11,94	76,5	88,30	M2	7a
45	-54,00	-45,00	34,22	10,30	7,90	81,4	88,30	M3	7a
46	11,00	7,00	35,74	7,37	10,91	80,4	88,20	M4	7a
47	-45,50	54,50	75,62	8,11	9,02	73,1	88,30	M5	7a
48	-45,00	51,00	39,56	8,18	10,67	87,3	88,20	M6	7a
49	-39,00	-24,00	32,92	8,00	13,22	105,7	88,30	M7	7a
50	-32,00	45,00	38,25	6,74	13,05	84,4	88,20	M8	7a
51	-23,00	-11,00	49,44	6,24	15,87	99,0	88,30	M9	7a
52	-18,00	39,00	49,25	6,32	15,50	98,0	88,20	M10	7a
53	-15,00	-21,00	70,87	6,27	15,60	97,8	88,30	M12	7a
54	-8,00	12,00	60,80	7,06	12,75	90,0	88,20	M13	7a
55	-1,00	1,00	73,89	6,97	13,08	91,17	88,30	M14	7a
56	-44,20	-4,50	11,20	6,43	16,80	108,0	88,30	C1	8a
57	42,32	-7,80	28,30	6,50	16,41	107,6	88,50	C2	8a
58	29,55	-7,37	29,70	12,30	9,13	117,8	88,50	C4	8a
59	-9,50	51,50	38,29	6,55	13,21	86,5	88,40	C31	8a
60	-49,58	23,25	44,02	8,55	6,84	58,5	88,40	C39	8a
61	-4,00	29,67	81,56	7,40	11,89	88,0	88,40	C40	8a
62	-15,26	0,90	70,88	6,78	13,10	88,8	88,60	C44	8a
63	-14,00	-11,67	11,58	8,88	9,42	83,6	88,50	C53	8a
64	-66,83	-16,67	16,82	7,64	4,13	69,7	88,40	C62	8a
65	-23,83	-17,83	30,81	7,08	12,43	88,0	88,50	C64	8a
66	-67,33	2,00	24,40	11,17	8,32	92,9	88,40	C80	8a

1	2	3	4	5	6	7	8	9	10
67	-37,95	8,08	25,25	11,70	6,60	77,6	88,40	C81	8a
68	-20,00	9,67	24,19	14,09	7,21	101,6	88,40	C83	8a
69	-11,42	14,56	91,31	9,30	9,94	92,4	88,40	C84	8a
70	-2,08	-5,75	31,78	12,20	7,42	90,5	88,60	C91	8a
71	-39,83	-17,33	105,12	9,57	8,93	89,0	88,50	C94	8a
72	-22,25	-20,70	34,69	11,44	9,23	110,2	88,50	C95	8a
73	-32,45	-21,37	46,95	7,85	13,13	110,5	88,50	C99	8a
74	-11,30	-43,00	69,78	17,27	6,64	114,7	88,60	C102	8a
75	-4,00	-32,50	77,46	20,66	5,73	118,4	88,60	C104	8a
76	-26,73	2,00	19,08	7,29	12,18	88,8	88,70	R1	9a
77	-24,50	2,35	11,16	8,59	10,44	89,7	88,70	R2	9a
78	-26,80	9,33	15,89	9,05	11,46	103,7	88,70	R4	9a
79	-10,39	9,67	105,29	7,84	9,76	76,5	88,70	R5	9a
80	-20,33	-27,17	104,63	7,42	10,50	77,9	88,70	R6	9a
81	-19,63	-31,50	49,49	12,72	7,01	89,2	88,70	R7	9a
82	-19,25	-31,67	46,53	12,92	7,01	88,9	88,70	R9	9a
83	-4,00	-31,67	56,40	17,37	6,90	119,8	88,70	R10	9a
84	-45,00	22,85	25,28	7,35	12,60	92,6	88,80	R11	9a
85	-41,17	24,00	27,44	7,30	15,07	109,8	88,80	R12	9a
86	-42,17	20,42	25,37	7,21	14,46	104,2	88,80	R13	9a
87	-40,17	19,00	20,82	7,22	16,75	120,9	88,80	R14	9a
88	-38,00	16,00	19,73	7,47	14,32	107,0	88,80	R15	9a
89	-42,83	7,17	18,08	7,00	13,77	92,9	88,70	R16	9a
90	-39,75	9,25	13,58	8,15	12,10	98,6	88,70	R17	9a
91	-32,00	6,42	11,21	7,24	12,05	87,2	88,70	R18	9a
92	-39,17	12,00	21,62	7,31	12,40	90,6	88,70	R20	9a
93	-2,63	9,47	12,81	7,43	10,84	80,5	88,80	V1	10a
94	-4,17	16,48	72,00	7,41	9,80	77,5	88,80	V5	10a
95	-4,83	-4,67	40,60	10,34	8,34	86,2	88,80	V8	10a
96	-3,27	16,77	71,25	8,23	9,66	79,5	88,70	V15	10a
97	-4,47	20,92	67,79	6,54	14,90	97,4	88,80	V16	10a
98	-4,00	12,83	37,48	5,12	17,12	97,24	88,90	T18	11a
99	-2,67	49,50	46,24	10,73	10,56	113,4	89,00	T20	11a
100	-16,25	14,67	36,89	7,95	10,60	84,3	88,90	T24	11a
101	-20,30	10,42	28,26	12,39	7,21	89,3	88,90	T26	11a
102	-22,00	32,67	44,34	6,29	17,70	107,8	89,00	T27	11a
103	-30,92	13,17	57,28	7,34	12,50	91,7	88,90	T28	11a
104	-40,92	26,50	31,31	7,36	12,88	97,8	89,00	T36	11a
105	-45,95	12,60	18,83	6,83	17,30	118,2	88,90	T50	11a
106	-4,08	-13,67	98,15	9,19	8,60	74,0	88,90	T69	11a
107	-17,33	39,50	37,76	6,46	16,65	107,6	89,00	T71	11a
108	-38,67	42,00	48,51	8,97	9,40	84,3	89,00	T72	11a

1	2	3	4	5	6	7	8	9	10
109	-40,58	36,42	37,79	8,07	10,00	81,0	89,00	T73	11a
110	-39,53	36,08	47,53	7,98	9,75	75,8	89,00	T74	11a
111	-39,72	34,50	32,87	7,09	11,45	81,2	89,00	T75	11a
112	-19,30	38,50	44,07	6,08	17,91	108,9	89,00	T79	11a
113	-18,70	40,37	46,80	6,39	16,85	107,7	89,00	T80	11a
114	-59,00	10,00	30,81	5,77	17,55	101,3	88,90	T82	11a
115	-42,00	34,00	37,14	6,47	18,39	119,0	89,60	T105	11a
116	-47,50	12,50	33,94	6,14	18,35	112,7	88,90	T106	11a
117	-14,00	-22,00	78,35	6,39	19,45	124,0	88,90	T107	11a
118	-13,17	2,75	67,65	6,78	19,11	124,8	88,90	T108	11a
119	-20,58	-10,67	60,07	6,59	15,30	100,8	89,30	S2	12a
120	-2,33	-12,92	47,77	10,04	8,66	86,9	89,30	S4	12a
121	-43,33	-2,33	35,00	5,33	19,60	104,5	89,30	S5	12a
122	-23,17	-3,33	34,83	6,36	15,00	95,4	89,30	S6	12a
123	-1,48	0,47	89,85	6,90	13,88	95,8	89,30	S8	12a
124	-11,43	-41,02	95,08	13,82	6,90	95,4	89,30	S9	12a
125	-64,55	7,00	21,87	6,70	15,60	104,5	89,30	S10	12a
126	-62,05	18,87	27,03	5,45	12,44	95,0	89,30	S11	12a
127	-19,57	-11,32	53,50	6,38	14,71	93,8	89,30	S13	12a
128	-1,45	0,02	88,32	6,92	19,20	133,0	89,10	P5	13a
129	-1,93	-3,93	110,00	10,50	11,10	116,5	89,10	P6	13a
130	-22,10	-3,52	27,26	6,74	15,80	105,1	89,20	P7	13a
131	-36,57	-2,98	33,13	5,75				P8	13a
132	-43,48	-1,97	24,35	5,55	19,20	106,6	89,20	P9	13a
133	-13,00	1,00	63,67	6,85	14,45	90,7	89,10	P18	13a
134	-27,17	3,47	24,33	7,23	10,88	78,7	89,10	P19	13a
135	-42,33	1,50	32,35	5,54	18,80	104,1	89,20	P22	13a
136	-27,45	0,62	22,15	7,35	18,75	137,8	87,50	P26	13a
137	-23,25	-3,08	43,16	6,52	15,32	99,9	89,20	P31	13a
138	-37,17	-3,17	32,80	5,66	18,92	107,1	89,20	P33	13a
139	-43,80	-2,47	30,11	5,25	19,01	104,0	89,20	P34	13a
140	-1,33	0,92	63,40	6,85	12,31	84,3	89,10	P37	13a
141	-9,00	5,00	63,32	5,50	18,52	101,9	89,10	P38	13a
142	-20,00	-0,50	37,61	7,00	13,53	94,7	89,10	P41	13a
143	-22,08	1,17	16,03	9,41	9,95	93,6	89,10	P42	13a
144	-23,25	-3,03	43,16	6,52	15,32	99,9	89,20	P43	13a
145	-43,92	-2,33	27,67	5,26	17,81	93,0	89,20	P46	13a
146	-1,33	0,42	87,22	6,94	10,16	70,5	89,10	P49	13a

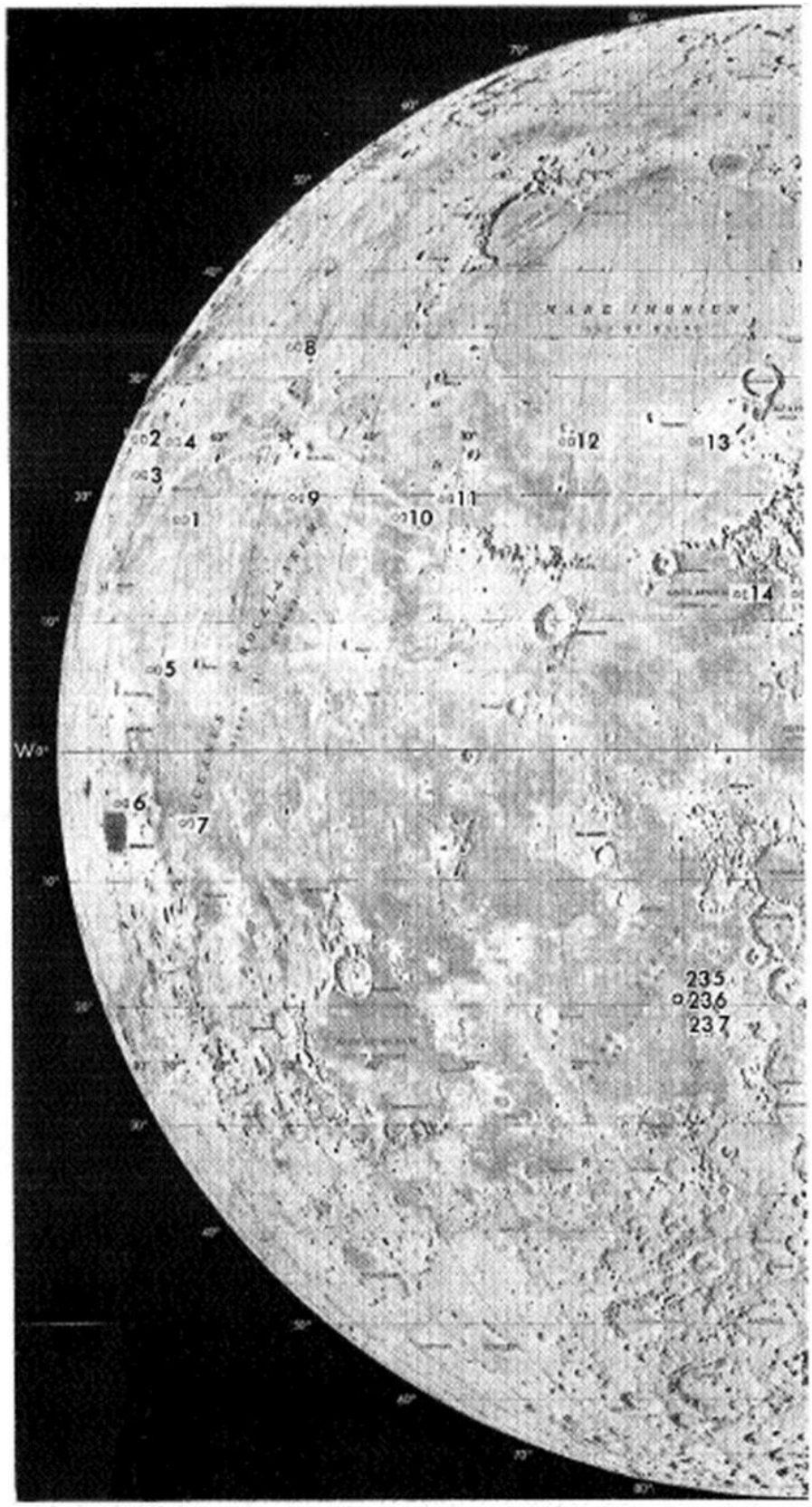

Figure 4a. Locations of dark albedo sites on the lunar disk.

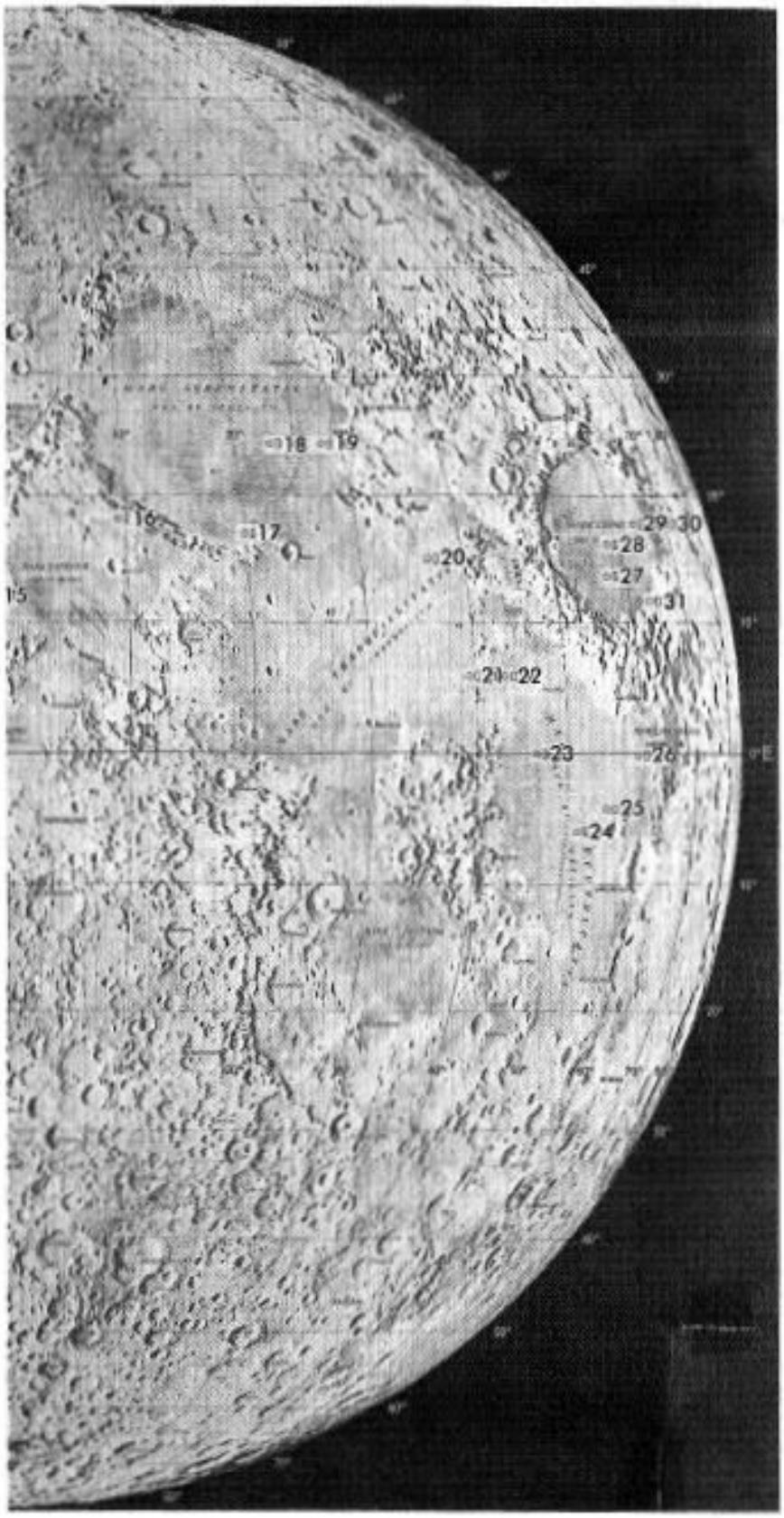

Figure 4b. Locations of dark albedo sites on the lunar disk.

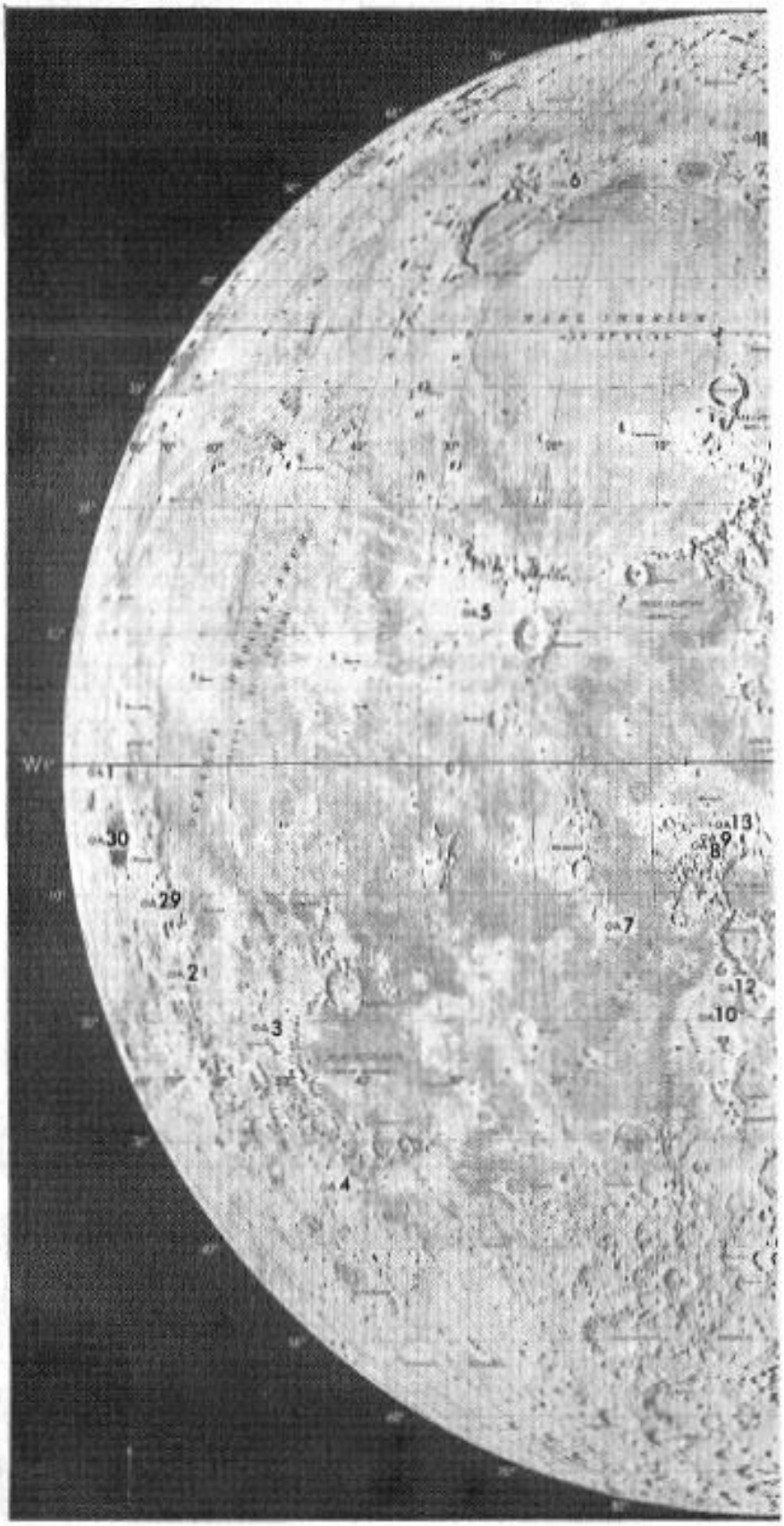

Figure 5a. Locations of average albedo sites on the lunar disk.

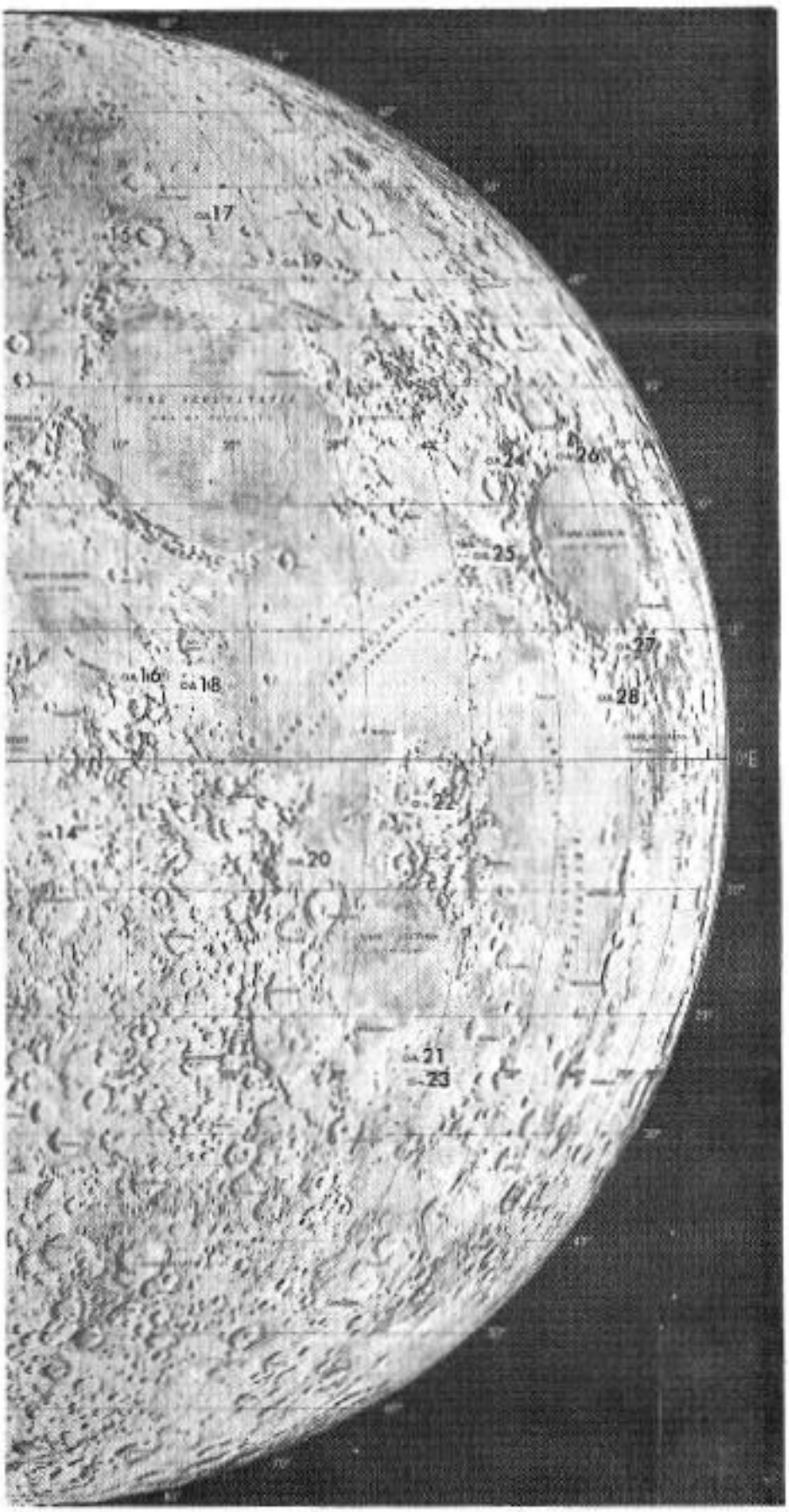

Figure 5b. Locations of average albedo sites on the lunar disk.

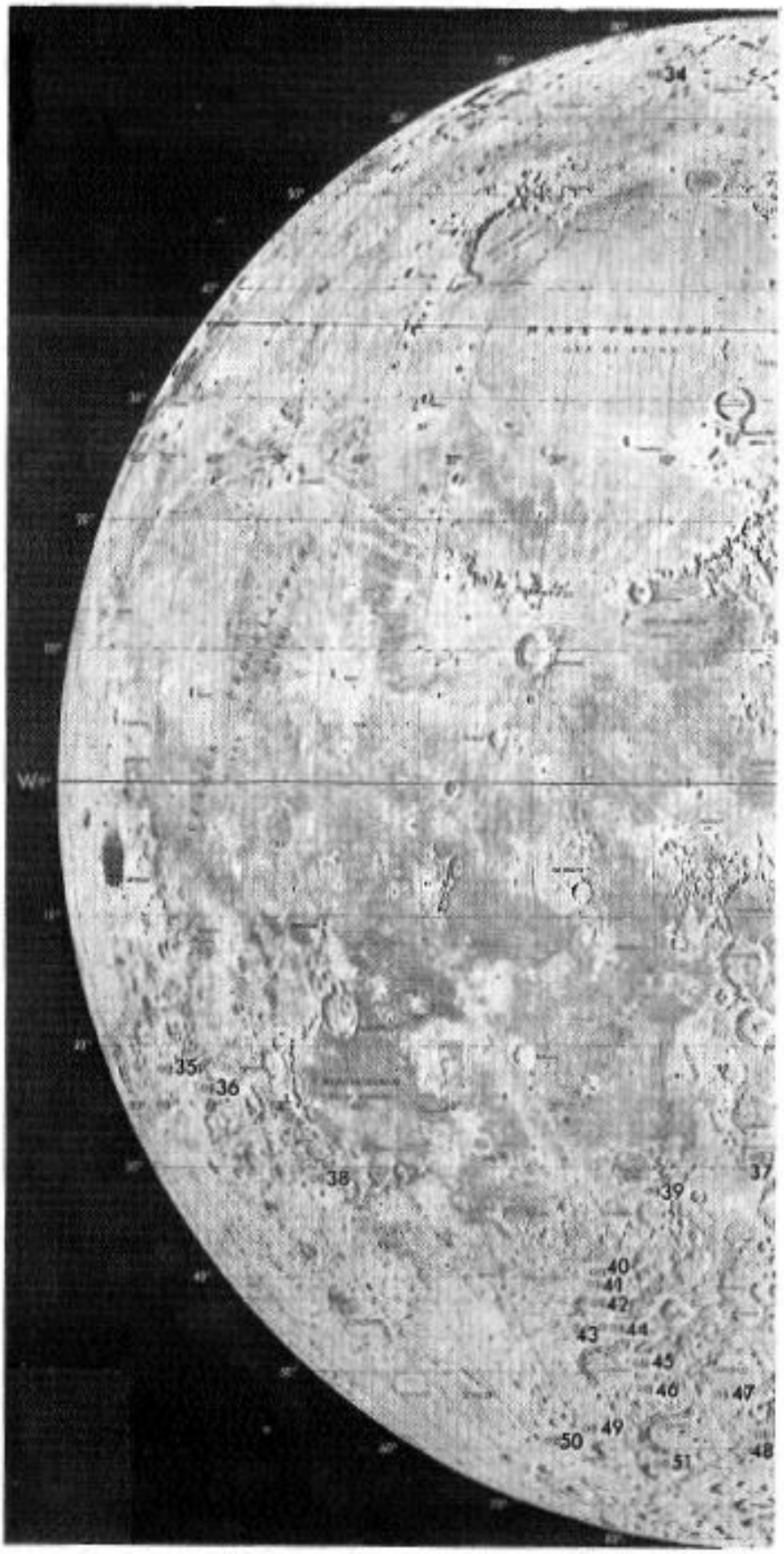

Figure 6a. Locations of bright albedo sites on the lunar disk.

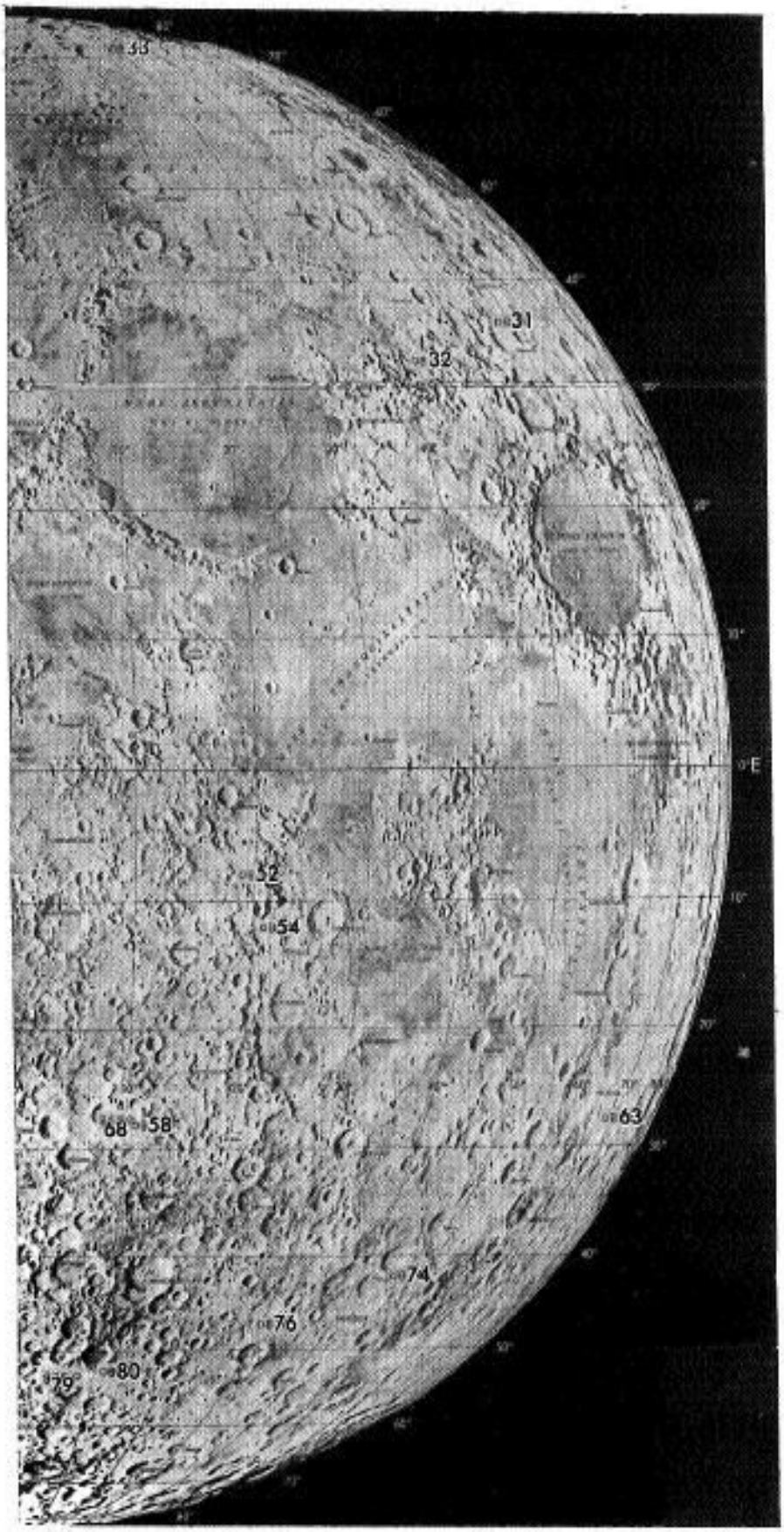

Figure 6b. Locations of bright albedo sites on the lunar disk.

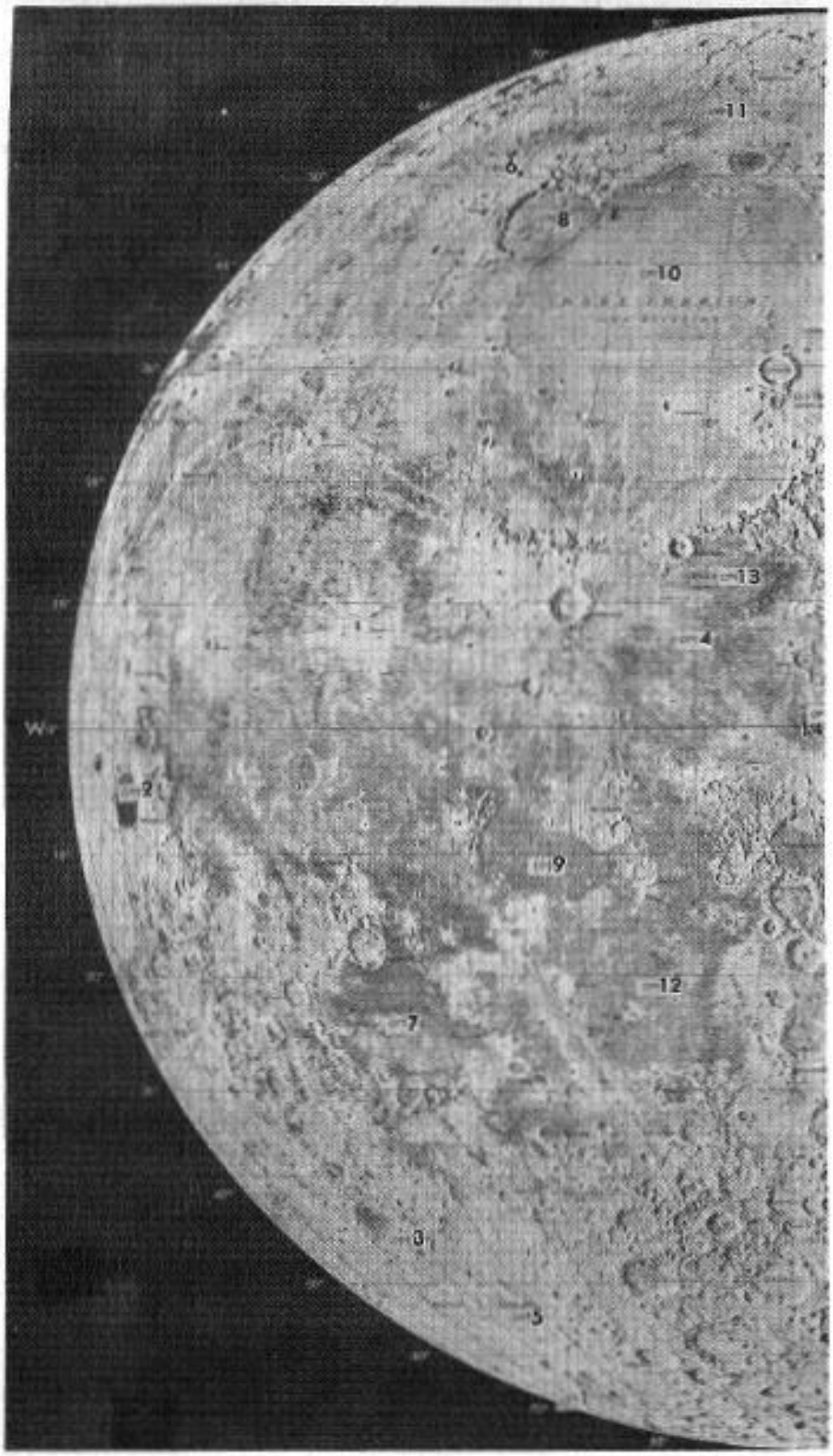

Figure 7a. Locations of mare sites on the lunar disk.

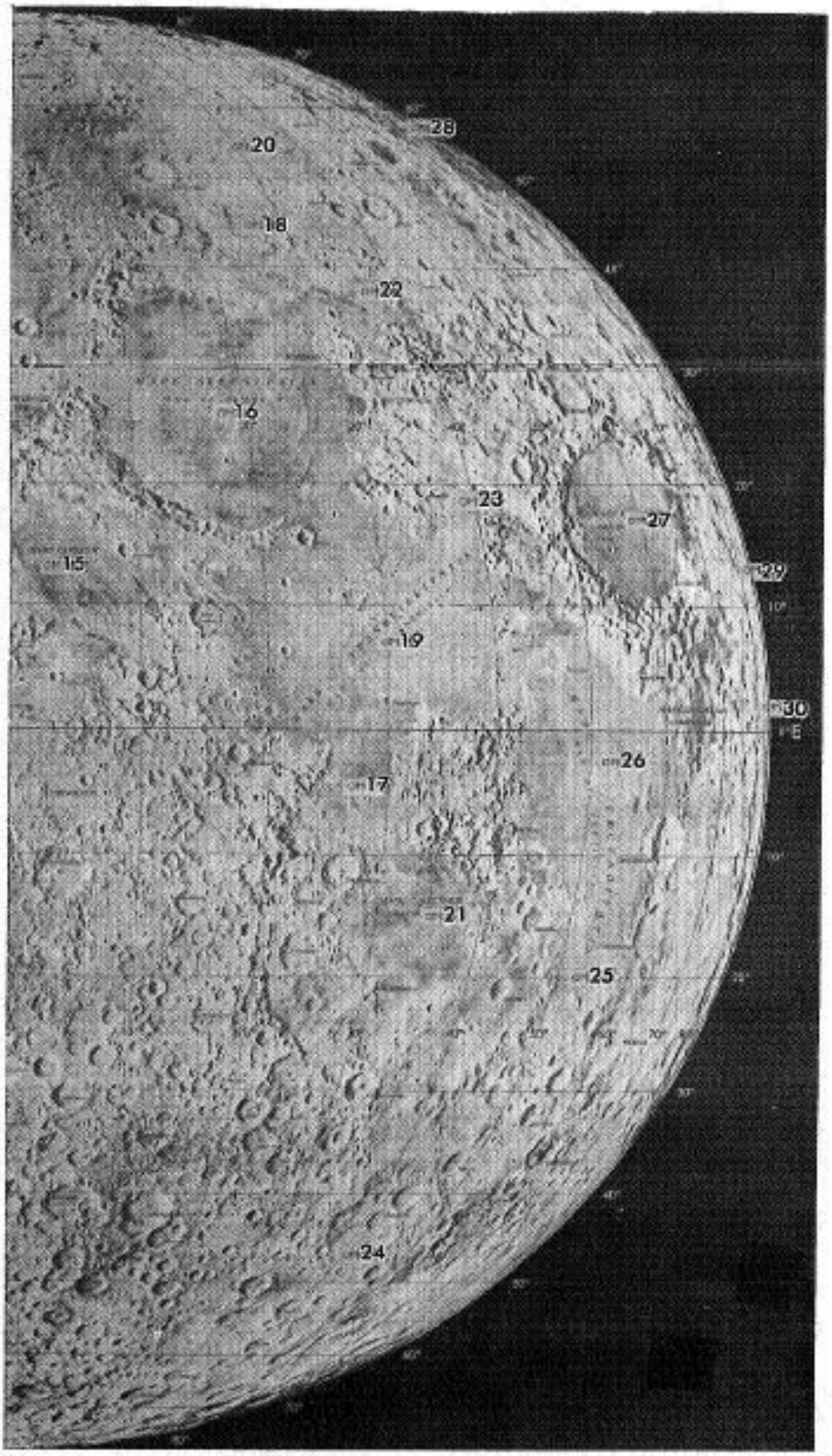

Figure 7b. Locations of mare sites on the lunar disk.

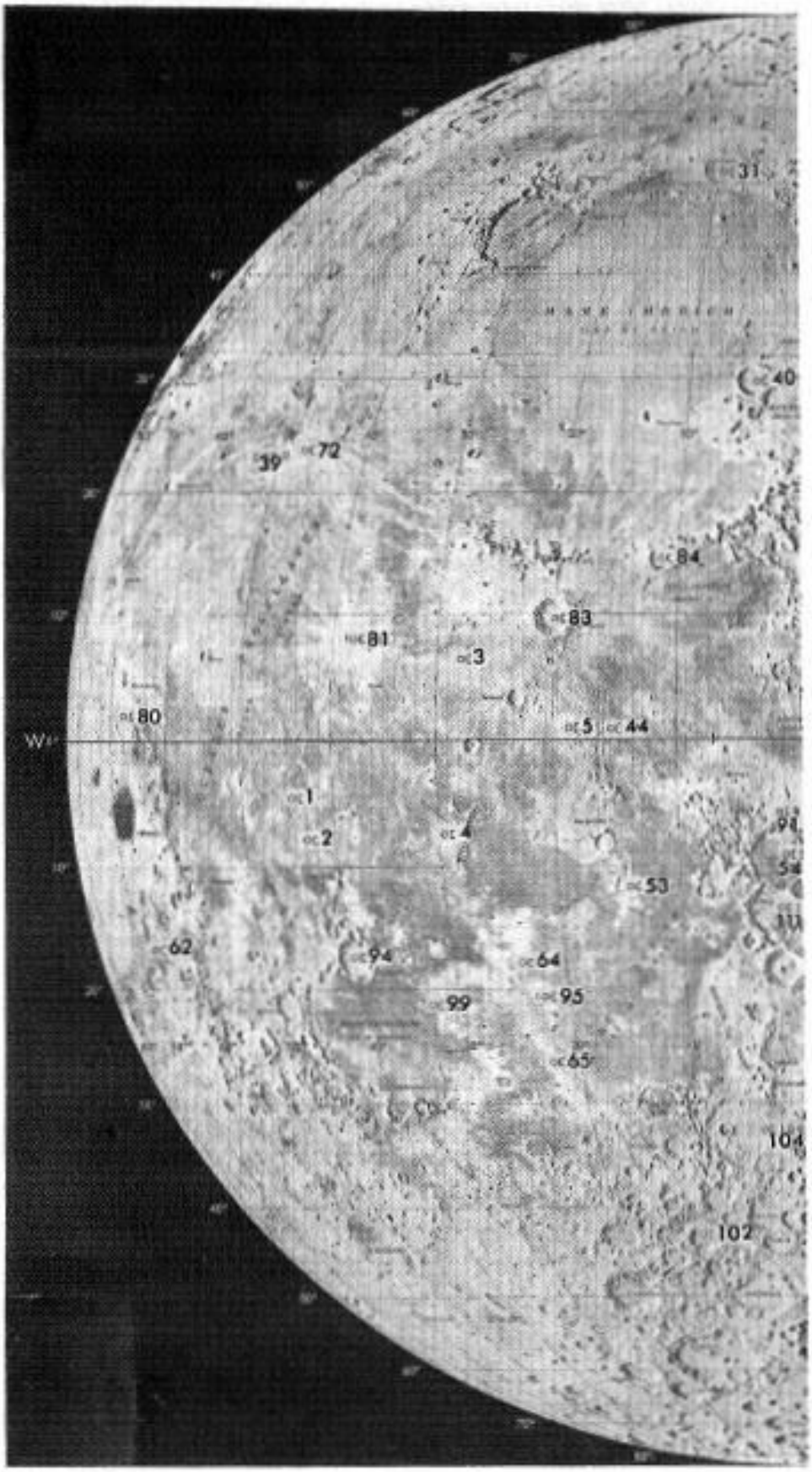

Figure 8a. Locations of crater sites on the lunar disk.

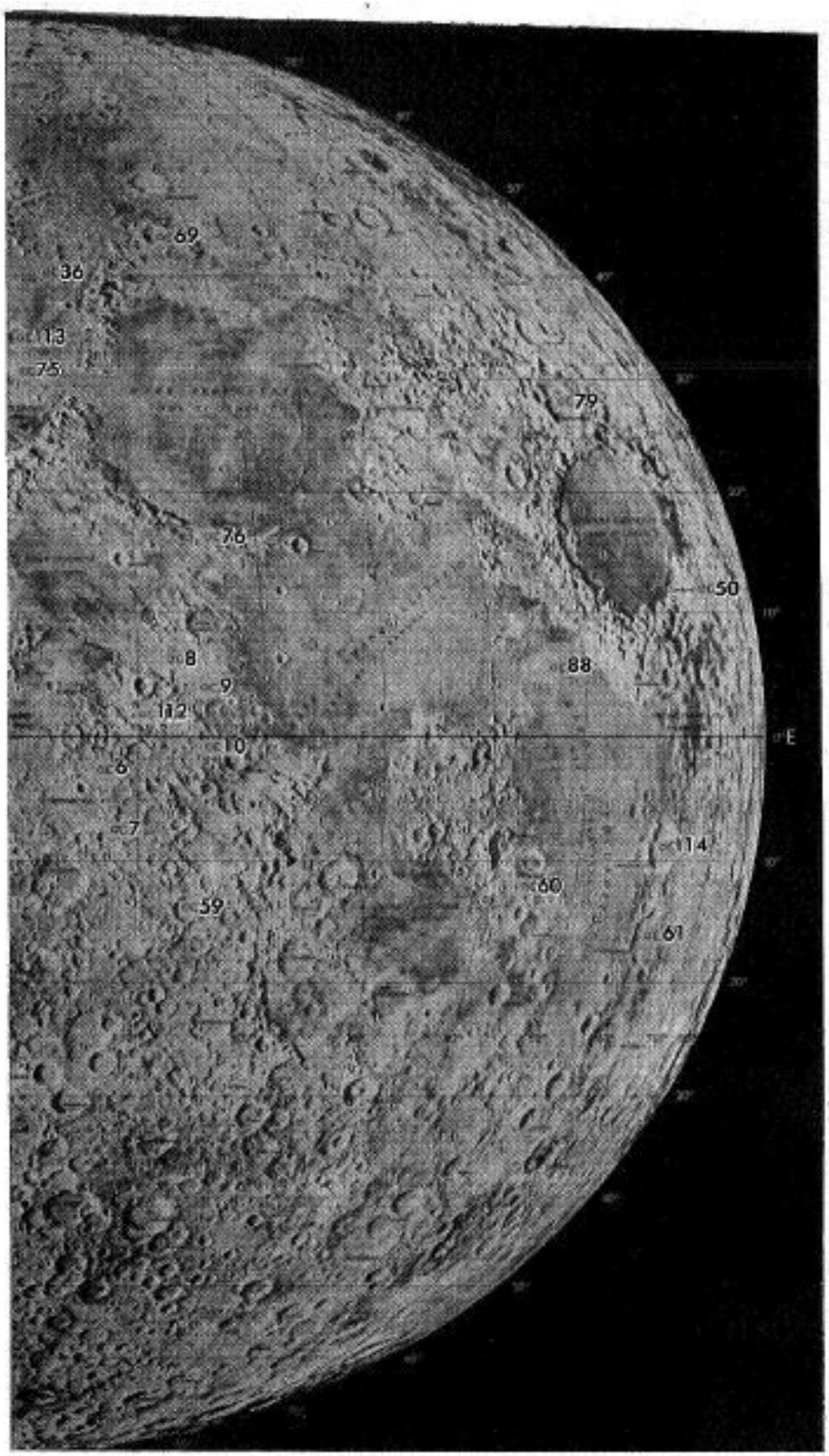

Figure 8b. Locations of crater sites on the lunar disk.

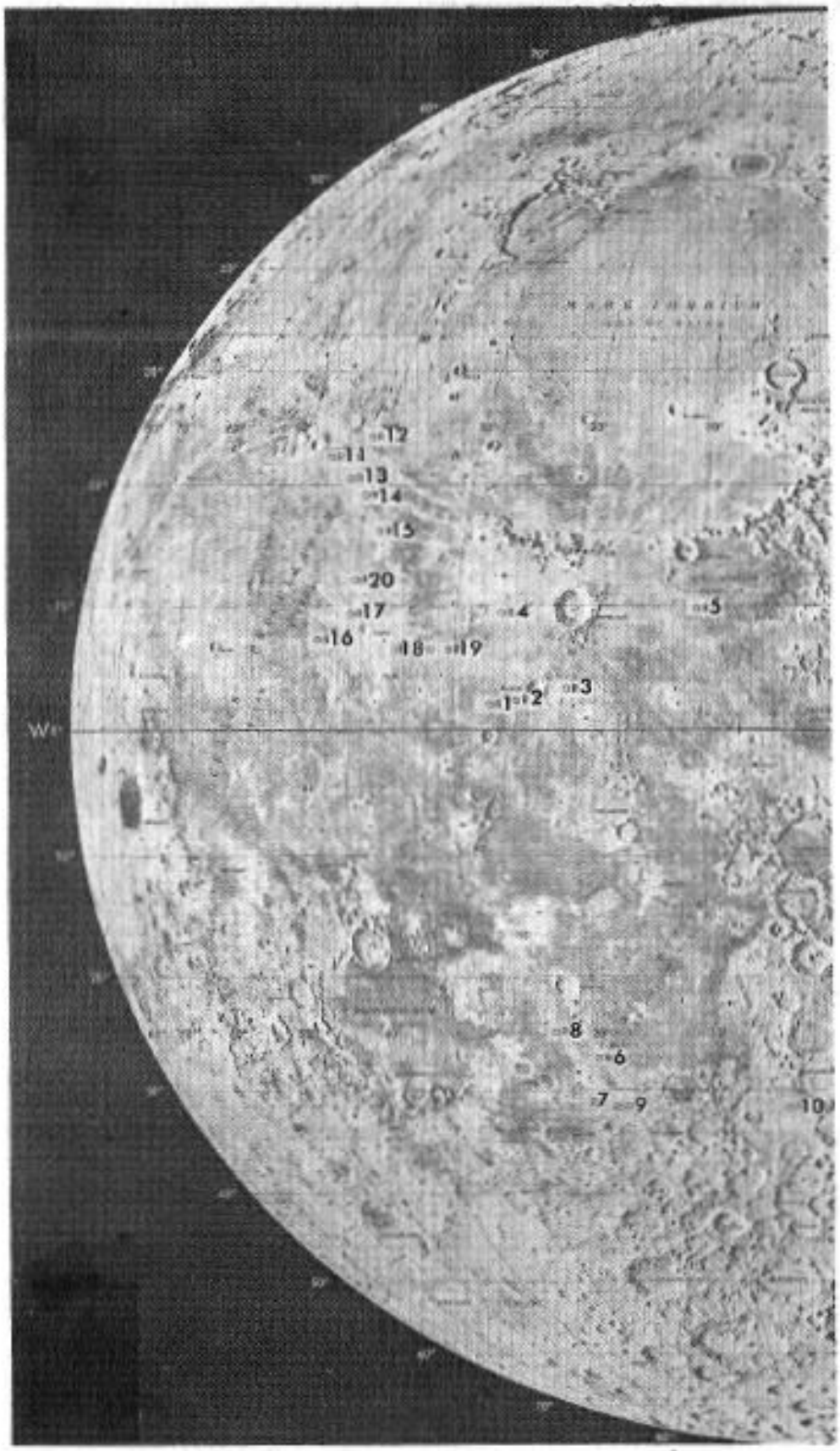

Figure 9a. Locations of ray sites on the lunar disk.

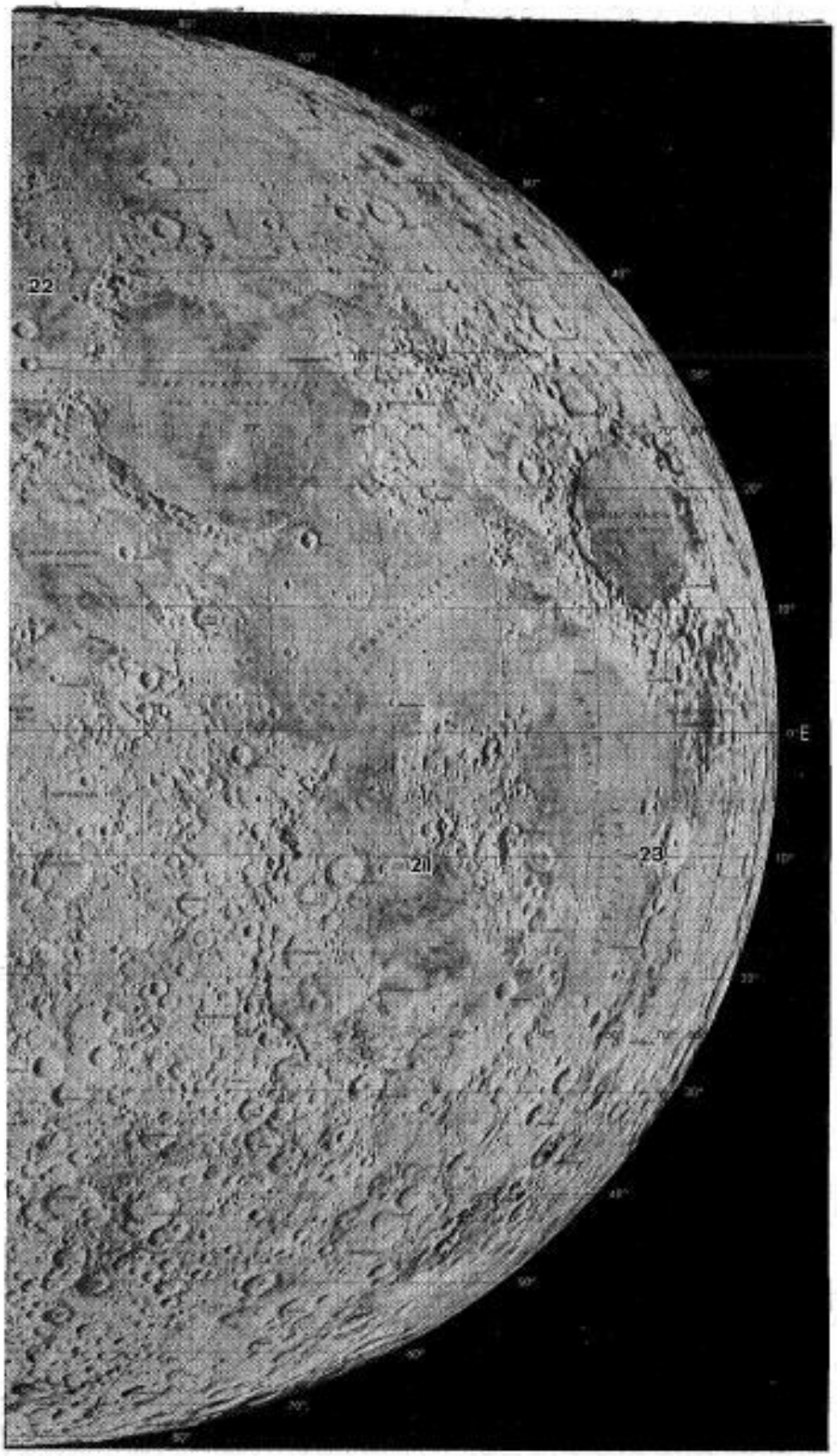

Figure 9b. Locations of ray sites on the lunar disk.

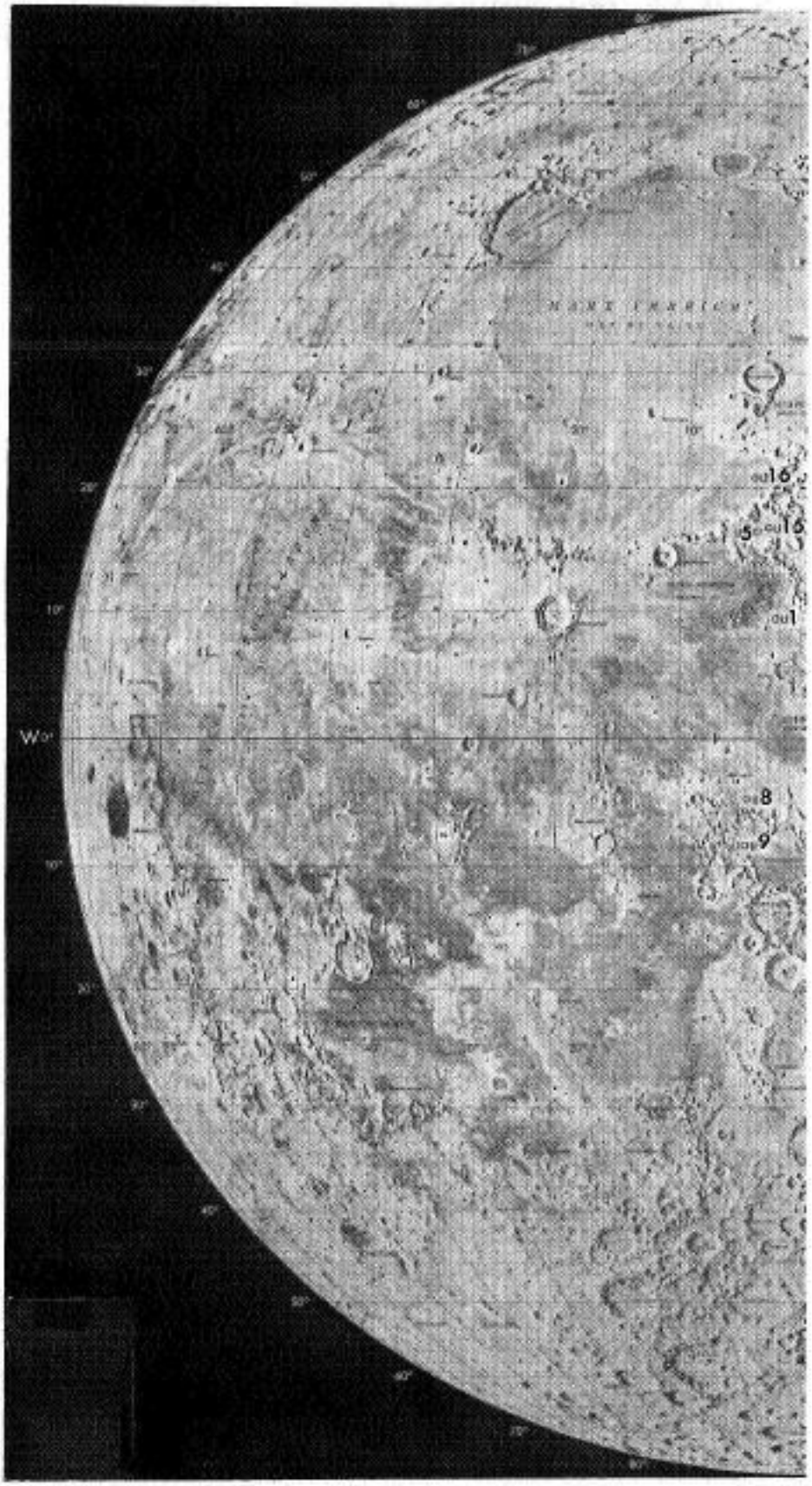

Figure 10a. Locations of upland sites on the lunar disk.

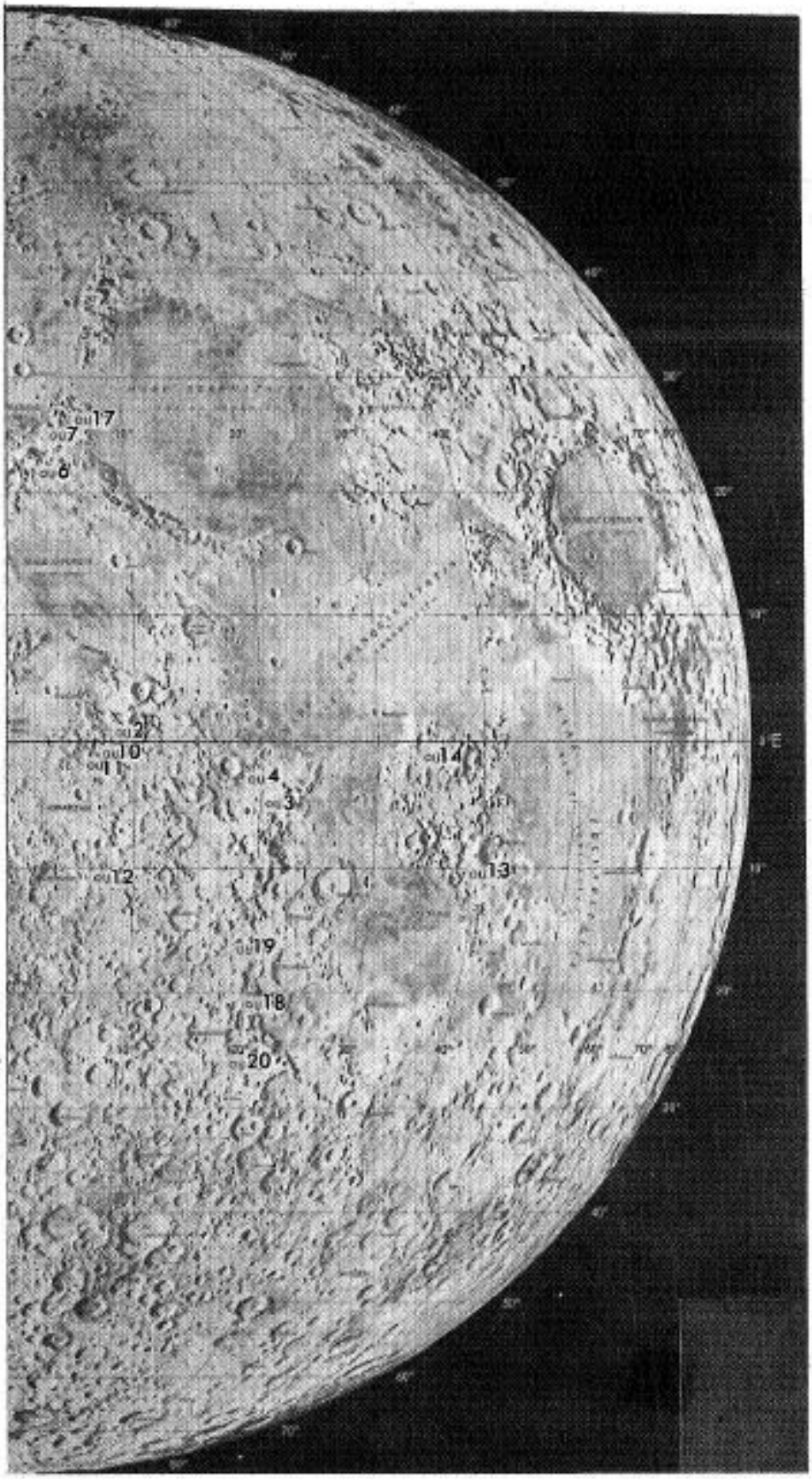

Figure 10b. Locations of upland sites on the lunar disk.

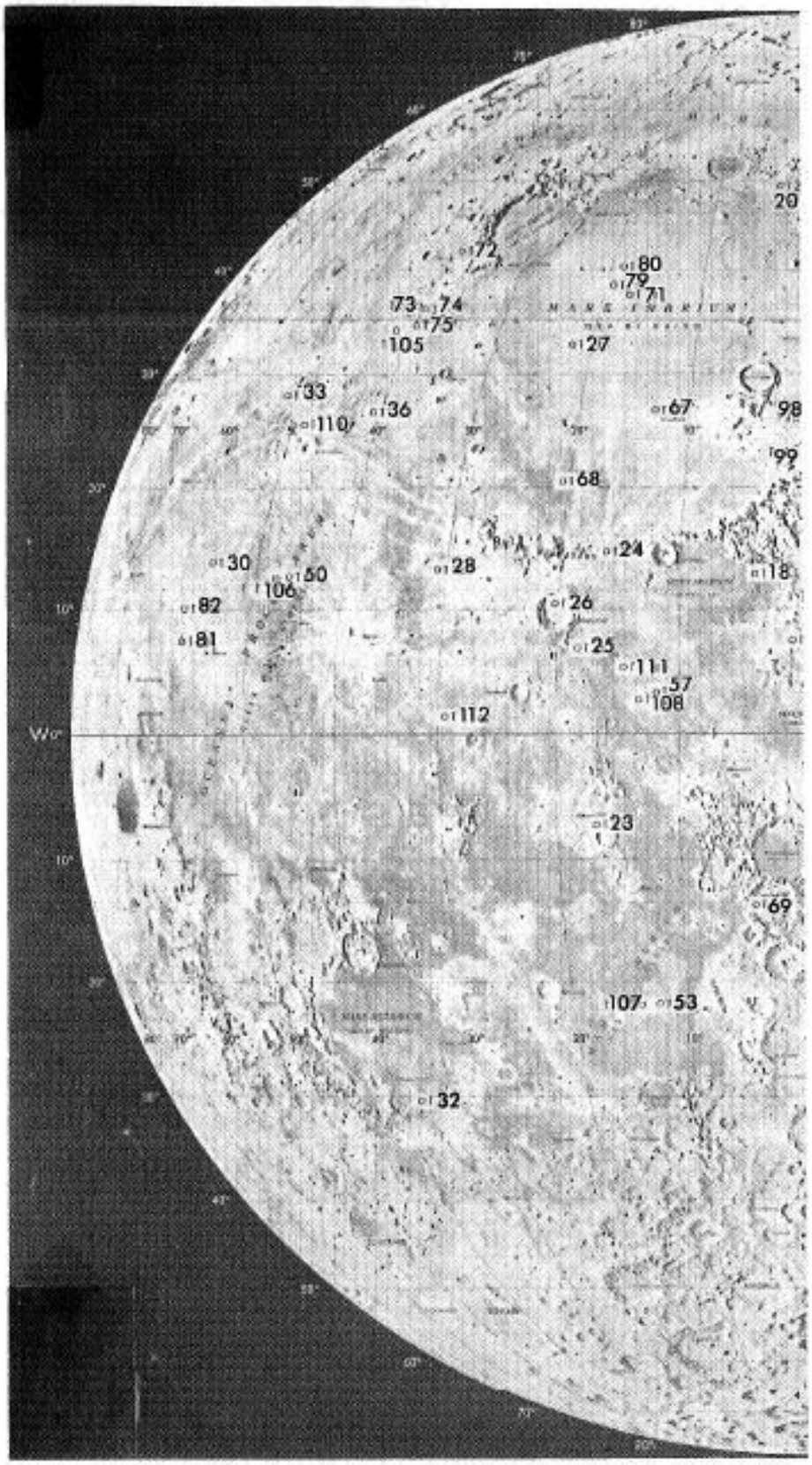

Figure 11a. Locations of scientific sites on the lunar disk.

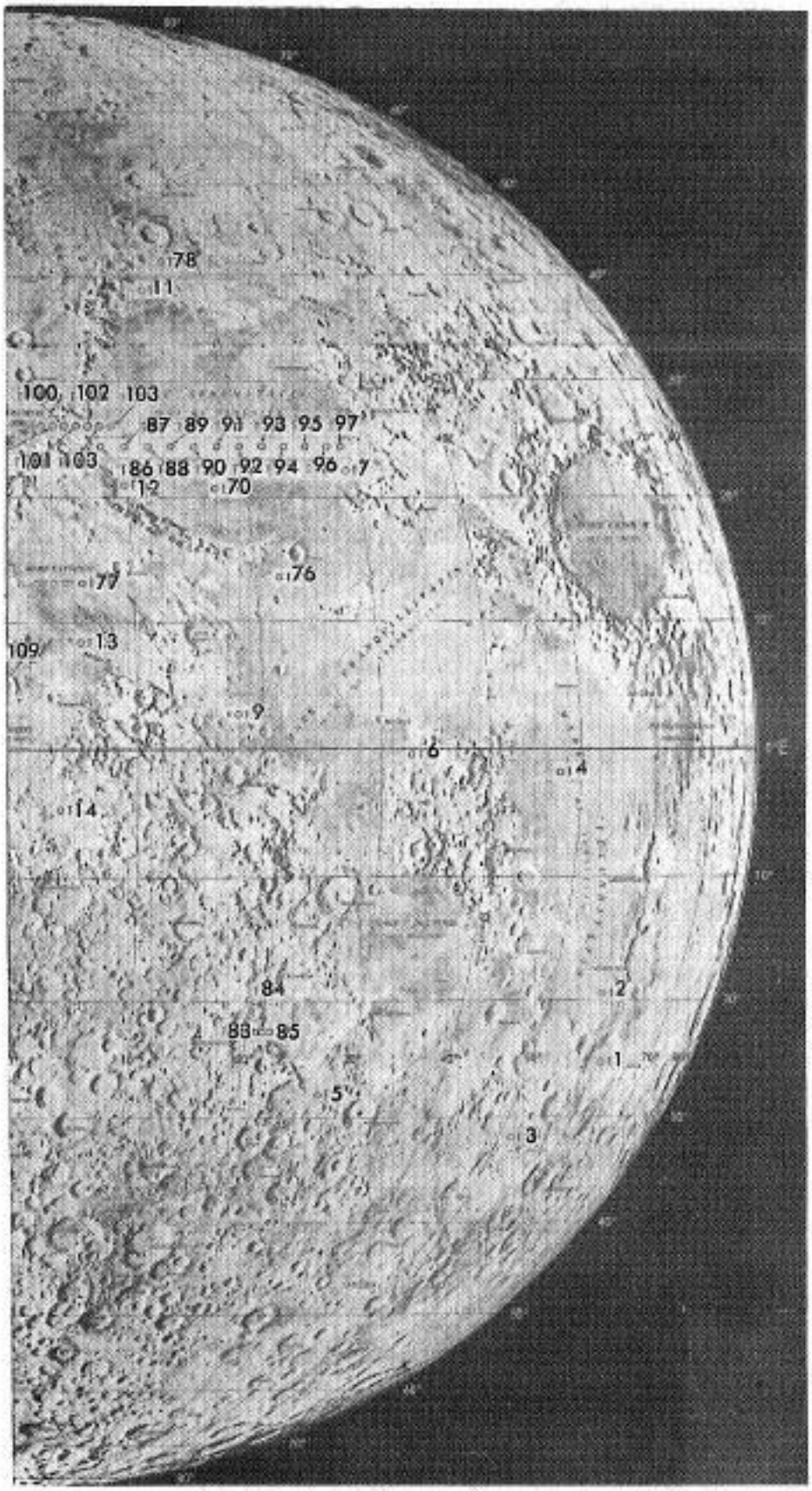

Figure 11b. Locations of scientific sites on the lunar disk.

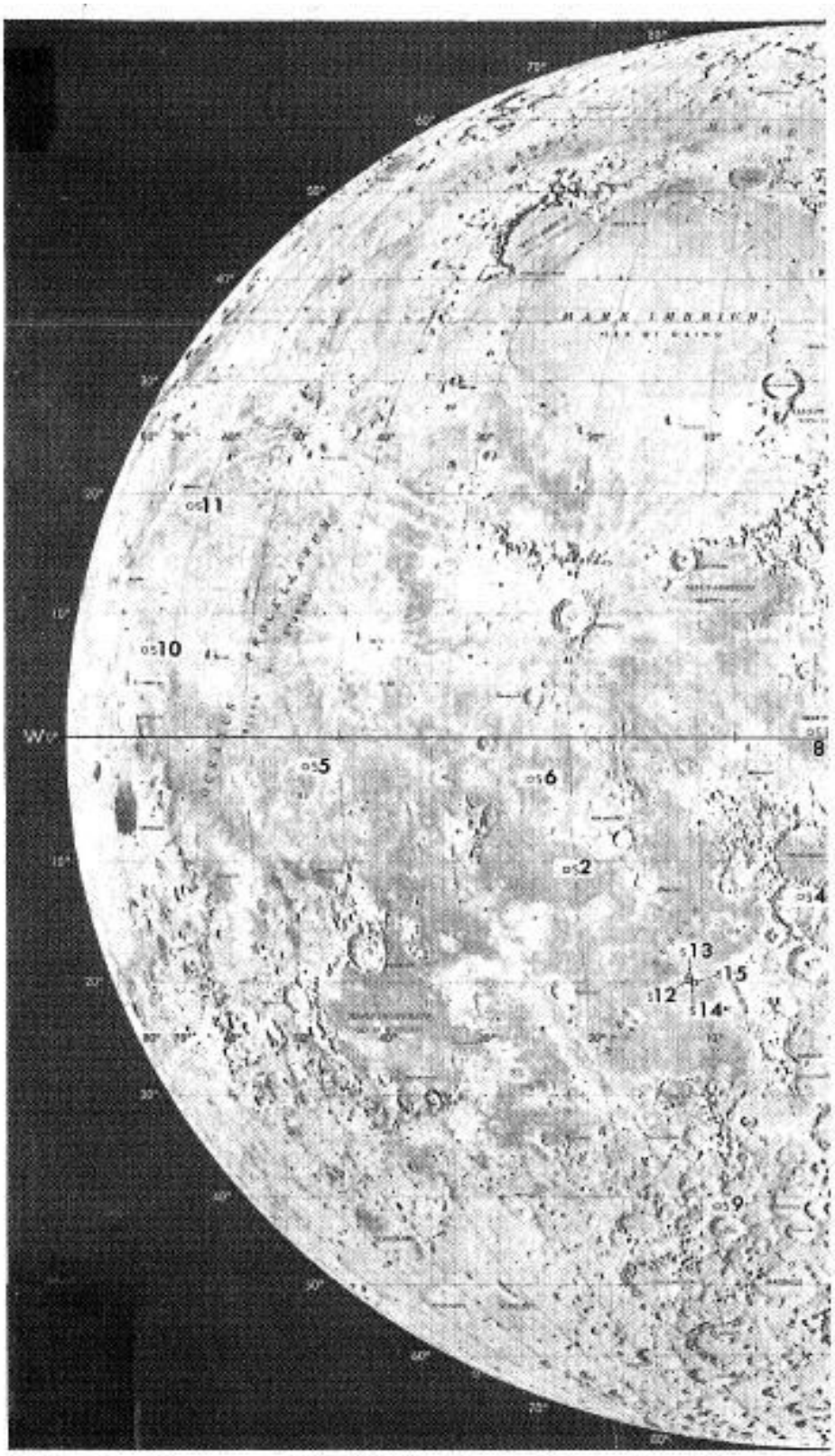

Figure 12a. Locations of spacecraft sites on the lunar disk.

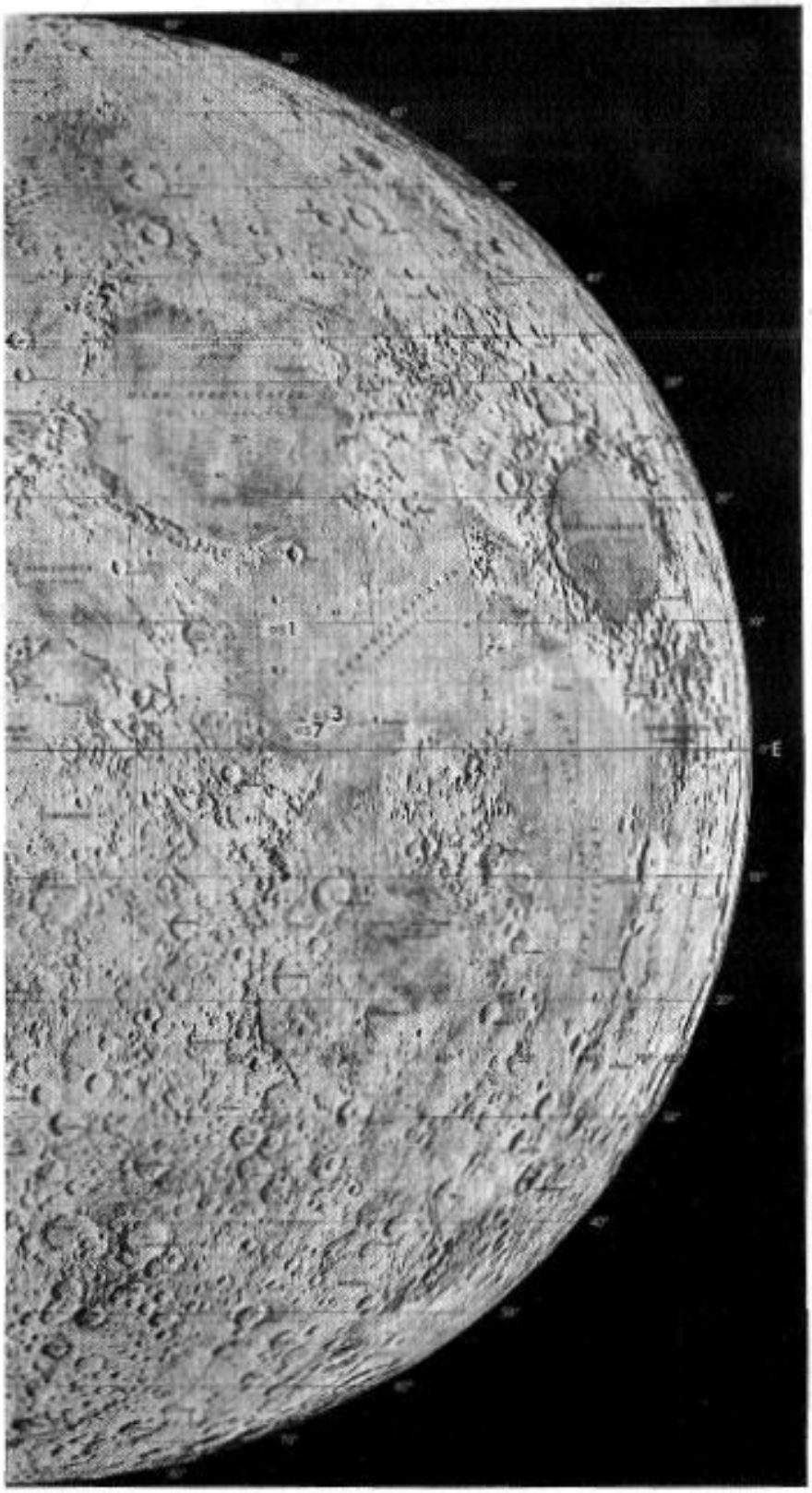

Figure 12b. Locations of spacecraft sites on the lunar disk.

Figure 13a. Locations of Apollo sites on the lunar disk.

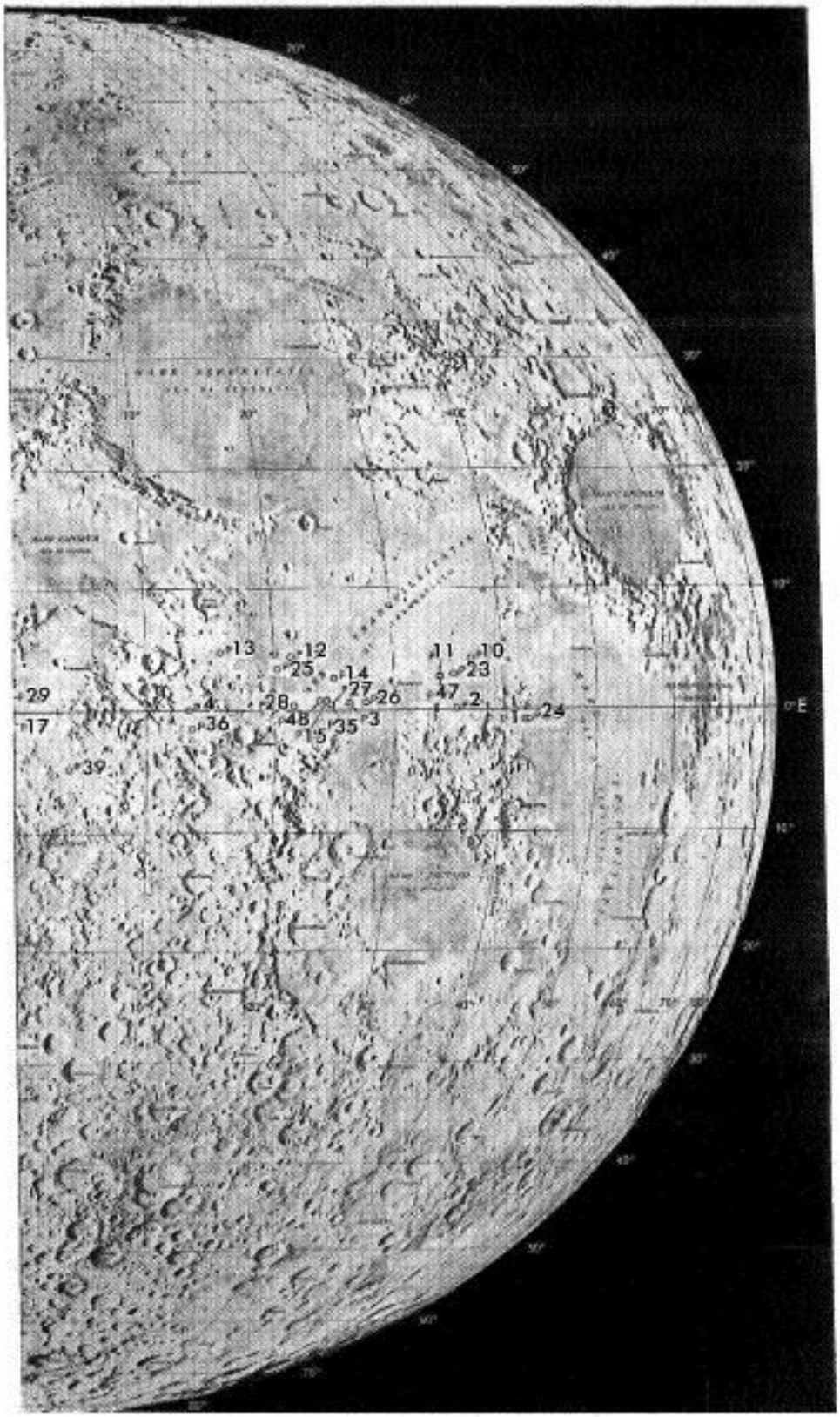

Figure 13b. Locations of Apollo sites on the lunar disk.

Astronomy & Astrophysics (Caucasus) 5, (2020) (37-51)

CATALOG KVARATSKHELIA OF EXTREME VALUES OF THE DEGREE OF POLARIZATION FOR 100 ARES OF THE LUNAR SURFACE

O.I. KVARATSKHELIA

E. Kharadze National Astrophysical Observatory

Email: kvara_otar@mail.ru

At the Abastumani Astrophysical Observatory, for 10 years (1976-1985), polarimetric observations of 100 areas of the lunar surface. The observations (with 40 cm refractor) were carried out with interference filters with the following effective wavelengths: 0.415 μm (half-width of transmission 0.017 μm); 0.433(0.009); 0.448(0.012); 0.468(0.012); 0.533 (0.016); 0.641 (0.009); 0. 670 (0.009); 0.704 (0.015); 0.783 (0. 011); and without filter (BF) - in integrated light (0.38-0.80 microns). The electronic-optical part of the polarimeter and the principle of its operation, as well as the method of observation and data processing, can be found in detail in the monograph by O. Kvaratskhelia [1]. The accuracy of the data given in the monograph was often verified by repeated observations in 2005-2009. on the same telescope and with the same equipment [8 - 10].

Table 1 gives the names and selenographic coordinates (λ - longitude, β - latitude) of the centers, measured by us objects of the lunar surface in accordance with the complete map of the Moon [2]. The same areas with the corresponding numbers are marked with crosses on the illustrative map of the Moon (see Fig. 1).

Below, in the form of a catalog, we present the obtained values of the maximum polarization (Pmax) values for the 100 areas of the lunar surface we measured in five light wavelengths. This catalog also contains the minimum values of the degree of polarization (Pmin) of the same objects. Measurements in the range 0.38-0.80 μm were performed in integral light using the same instrumentation system (telescope and polarimeter). Table 2 shows the albedo values for objects in

the catalog of O.I. Kvaratskhelia [1], taken from five different albedo maps of the Moon [3 - 7]. Table and catalog numbers correspond.

References

1. Kvaratskhelia O.I., Spectropolarimetry of the lunar surface and lunar soil samples. Bulletin Abastum. astrophysis. Observatory, 1988. No. 64, p. 312.

2. Complete map of the Moon, compiled under the guidance of Yu. N. Lipsky. M.Nauka. 1979.

3. Shorthill R.W., Saari J.M., Baird F.E., Le-Compte J.R. Photometric Properties of Selected Lunar Features.-NASA CR-1429, Washington. 1969.

4. Shevchenko V.V., On the nature of the albedo of the surface of the lunar ball. - Astron. J. 1974, 51, No. 5, 1064-1071.

5. Pohn H.A., Wildey R.L. A Photoelectric-photographic Study of the Normal Albedo of the Moon.-Geological Survey Professional Paper 599 E.1070, 20 p.

6. Evsyukov N.N., Albedo map of the visible hemisphere of the Moon. Naukova dumka. 1973.

7. Akimov L.A., Change in the brightness of lunar formations with phase. - Bulletin of KSU. 1982, no. 232, 12-22.

8. Kvaratskhelia O.I., International Scientific Conference ''Problems of Modern Astrofysics''report "Spectropolarimetry of the Moon''. Akhaltsikhe. 2015.

9. Kvaratskhelia O., Ivanidze R., Gigolashvili Sh. Spectropolarimetry of the Lunar Surface and Ground Samples. Astronomy and Astrophysics [Caucasus]1, 2016, pp.49-52.

10. Kvaratskhelia O., Chigladze R., et al. Multiparameter Atlas of the Moon. E.Kharadze Abastumani Astrophisical Odservatory. 1-180, 2019.

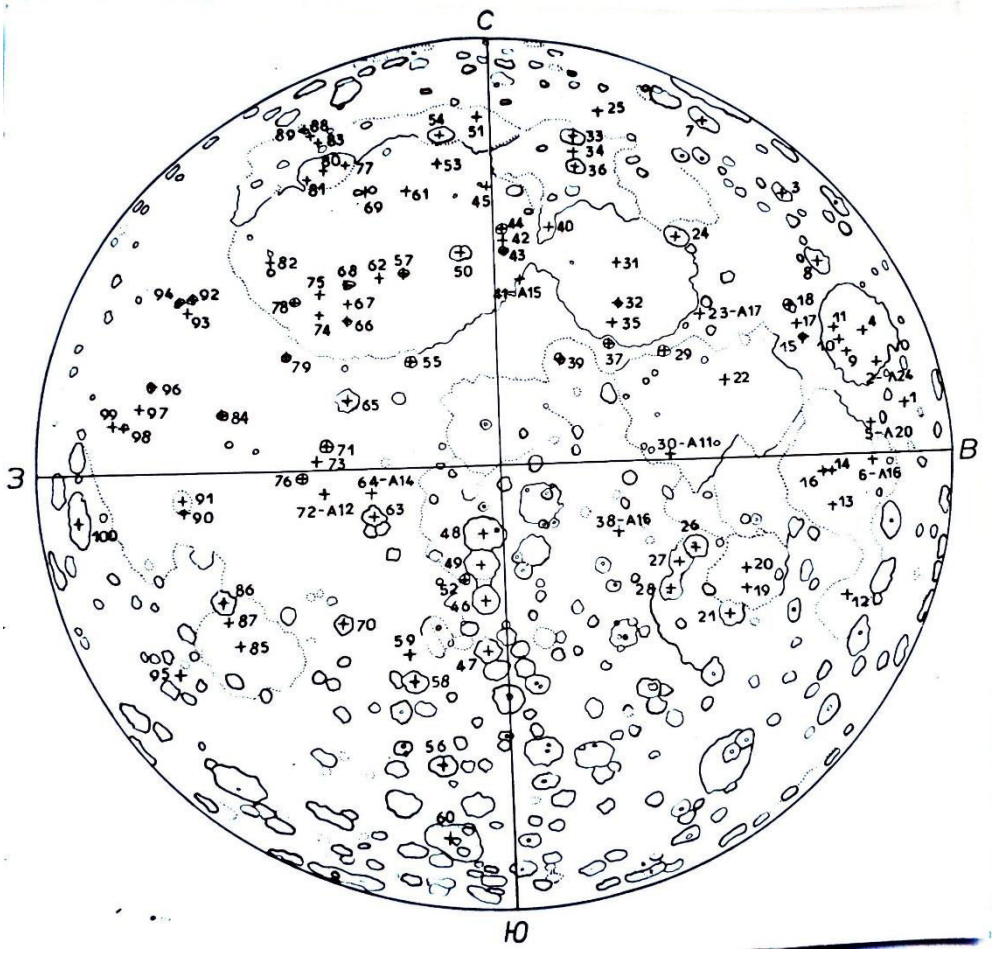

Figure: 1. Illustrative map of the Moon. The crosses indicate the centers of the surface areas we measured. The numbers of the crosses correspond to the numbers of the catalog in Table 1.

Table 1

N	Object no. according to Catalog of O.Kvaratskhelia	Selenographic		Diameter of measured area, arccec
		Longitude λ^0	Latitude β^0	
1.	Mare Undarum	+67.5	+7.0	7.5
2.	Landing sites "Luna-24"	+62.2	+12.8	15.1
3.	Messala C. (Crater)	+60.0	+39.0	7.5
4.	Mare Krisium (central part)	+59.0	+17.0	15.1
5.	Landing sites ("Luna-20")	+56.5	+3.5	15.1
6.	Landing sites "Luna-16"	+56.3	-0.7	15.1
7.	Endumion C	+56.3	+53.2	15.1
8.	CleomedesC	+55.8	+28.0	15.1
9.	Pikard C	+54.6	+14.4	1.5
10.	Mare Krisium (N Pikar)	+53.7	+16.3	7.5
11.	Peirse C	+53.2	+ 18.2	1.5
12.	Mare Fecunditatis (S parts)	+53.0	-18.0	7.5
13.	Mare Fecunditatis (SW parts)	+49.0	-8.0	7.5
14.	Messier C	+47.7	-1.8	1.5
15.	Proklus C	+47.0	+16.0	3.0
16.	Pikering C	+46.9	-2.0	1.5
17.	Continent part (NProklus)	+46.4	+18.2	7.5
18.	Macrobius C	+46.0	+21.0	7.5
19.	Rosse C	+35.0	-17.8	1.5
20.	Mare Nectaris(central part)	+33.5	-14.7	7.5
21.	Fracastorius C	+33.0	-21.0	15.1
22.	Mare Tranqnillitatis(central part)	+32.0	+11.0	7.5
23.	Landing sites ("Apollo-17")	+30.7	+20.2	7.5
24.	Posidonius C.	+30.0	+31.6	15.1

25.	Mare Frigorus(NE Galle)	+28.0	+56.0	7.5
26.	theophilins C	+26.4	-11.3	15.1
27.	Cyrilus C	+24.0	-13.0	15.1
28.	Catharina C	+23.7	-18.0	15.1
29.	Plinius C	+23.8	+15.0	3.0
30.	Landing sites “Apollo—11”	+23.5	+0.7	15.1
31.	Mare Serenitati s (central part)	+18.0	+28.0	7.5
32.	Bessel C	+17.8	+21.6	1.5
33.	Aristoteles C	+17.4	+50.0	15.1
34.	Continent part (N Eudocsus)	+17.0	+46.7	7.5
35.	Mare Serenitatis (N Bessel)	+17.0	+19.0	7.5
36.	Eudocsus C	+16.6	+43.7	`15.1
37.	Menelaus	+16.0	+16.0	3.0
38.	Landing site “Apollon-16”	+15.5	-9.0	15.1
39.	Manilius C	+9.3	+14.2	3.0
40.	Caucasus Montes	+9.0	35.0	7.5
41.	Landing sites “Apollon-15”	+3.6	+26.1	7.5
42.	Mare Imbrium(N Autoolykus)	+1.3	+32.0	7.5
43.	Autolikus C	+1.3	+30.5	7.5
44.	Aristillus C	+1.0	+33.7	7.5
45.	Mons Piton	-1.2	+40.5	1.5
46.	Arzachel C	-2.0	-18.5	7.5
47.	Purbach C	-2.0	-25.3	7.5
48.	Ptollemaus C	-2.2	-9.0	15.1
49.	Alphonsus C	-3.0	-13.2	15.1
50.	Archimedes	-4.0	+29.6	15.1
51.	Mare Frigorus (central part)	-4.0	+58.0	7.5
52.	Alpetragius C	-4.6	-16.0	3.0
53.	Mons Pico	-9.0	+45.4	1.5
54.	Plato C	-9.5	+51.5	15.1
55.	Eratosthenes C	-11.3	+14.5	7.5

56.	Tycho C	-11.3	-43.0	7.5
57.	Timocharis C	-13.0	+26.5	7.5
58.	Pitatus C	-13.5	-29.7	7.5
59.	Mare Nubium (central part)	-14.0	-24.5	7.5
60.	Klavius C	-14.7	-58.3	15.1
61.	Mare Imbrium(central part)	-15.0	+41.0	7.5
62.	M areImbrium(W Timocharis)	-16.5	+26.2	7.5
63.	Fra Mauro C	-17.0	-6.0	7.5
64.	loading sites “Apollon-14”	-17.5	-3.7	7.5
65.	Copernicus C	-19.8	+9.5	15.1
66.	Pytheas C	-20.5	+20.5	1.5
67.	Mare Imbrium (N pytheas)	-20.7	+23.0	7.5
68.	Lambert C	-20.8	+25.7	3.0
69.	Mare Imbrium (W Le Werrier)	-21.6	+40.2	7.5
70.	Bullialdus C	-22.2	-20.5	3.0
71.	Reinhold C	-22.8	+3.0	3.0
72.	Loading sites “Apollon-12”	-23.4	-3.2	7.5
73.	OcaenusProcellarum (SW Reinhold)	-25.0	+1.0	7.5
74.	Mare Imbrium (SE Euler)	-25.0	+21.5	7.5
75.	M areImbrium(NE Euler)	-25.0	+24.5	7.5
76.	Lancberg C	-26.7	-0.5	3.0
77.	Sinus Iridum (E part)	-29.0	+46.0	7.5
78.	Euler C	-29.2	+23.3	1.5
79.	Mayer C	-29.5	+15.5	1.5
80.	Sinus Iridum (central part)	-32.0	+44.5	7.5
81.	Sinus Iridum (W part)	-34.0	+42.5	7.5
82.	Mare Imbrium(N diophantus)	-34.5	+28.5	3.0
83.	Continent part (NW bianchini)	-37.5	+49.4	3.0
84.	Kepler C	-38.0	+8.0	3.0
85.	Mare Humorum(central part)	-39.0	-24.0	7.5
86.	Gassendi C	-39.7	-17.3	15.1

87.	Mere Humorum (S Gassendi)	-40.0	-20.0	15.1
88.	Mare Frigoris (SW Garpall)	-41.5	+51.3	7.5
89.	Garpall C	-43.5	+52.4	3.0
90.	Flamstiid C	-44.0	-4.5	1.5
91.	Oceanus Procellarum(N Flamstid)	-44.0	-3.2	7.5
92.	Aristarchus C	-47.4	+23.5	3.0
93.	Aristarchus Region	-48.5	+22.2	3.0
94.	Herodotus C	-49.6	+23.2	3.0
95.	Continent part (SW Gavendis)	-50.0	-27.5	7.5
96.	Marius C	-50.6	+11.8	3.0
97.	Oceanus Procellarum (SW Marius)	-53.0	+9,0	7.5
98.	Reiner	-55.0	+6.7	3.1
99.	Reiner	-58.5	+7.0	3.1
100.	Grimaldi (central part)	-68.0	-5.0	7.5

CATALOG KVARATSKHELIA. Maximum values of the degree of polarization(Pmax)

N	Pmax (4190Å)	lgPmax	Pmax (4480Å)	lgPmax	Pmax (5350Å)	lgPmax	Pmax (6400Å)	lgPmax	Pmax (Int)	lgPmax (Int)
1	2	3	4	5	6	7	8	9	10	11
1	12,5	1,10	11,5	1,06	10,0	1,00	9,5	0,98		
2	16,5	1,22	14,3	1,16	13,0	1,11	11,0	1,04	11,5	1,06
3	7,0	0,84	6,7	0,83	6,2	0,79	5,0	0,70		
4	16,0	1,20	15,0	1,18	12,0	1,08	10,0	1,00		
5	9,5	0,98	8,0	0,90	6,0	0,78	5,8	0,76	6,0	0,78
6	18,5	1,27	17,0	1,23	14,0	1,15	12,2	1,09	12,5	1,10
7	7,2	0,86			6,5	0,81				
8	8,0	0,90	7,7	0,89	6,7	0,83	6,0	0,78		
9	15,0	1,18	14,5	1,16	12,0	1,08	9,5	0,98	9,5	0,98
10	14,0	1,15	13,0	1,11	10,5	1,02	9,0	0,95	10,0	1,00
11	14,1	1,15	13,2	1,12	10,5	1,02	8,7	0,94	9,5	0,98
12	15,0	1,18	14,0	1,15	10,5	1,02	8,5	0,93		
13	17,5	1,24	16,0	1,20	14,0	1,15	11,3	1,05	12,0	1,08
14									10,0	1,00
15	6,3	0,80	5,2	0,72	4,0	0,60	3,7	0,57	3,8	0,58
16	16,4	1,21	15,2	1,18	12,5	1,10	10,7	1,03	11,0	1,04
17	7,5	0,88	7,0	0,84	6,0	0,78	4,8	0,68	5,2	0,72
18	8,8	0,94	8,0	0,90	7,0	0,84	6,3	0,80	6,0	0,78
19	12,7	1,10	12,0	1,08	10,0	1,00	8,0	0,90	7,0	0,84
20	13,0	1,11	12,5	1,10	10,3	1,01	8,0	0,90	9,0	0,95
21	9,7	0,99	9,0	0,95	8,5	0,93	6,9	0,86	7,0	0,84
22	20,7	1,32	18,2	1,26	16,5	1,22	13,5	1,13	14,0	1,15
23	12,0	1,08	11,0	1,04	9,8	0,99	7,8	0,89	7,5	0,88
24	9,5	0,98	8,9	0,93	7,5	0,88	6,5	0,81	6,5	0,81
25	13,5	1,13	13,0	1,11	10,0	1,00	8,8	0,94		
26	6,2	0,79	6,5	0,81	5,3	0,72	5,0	0,70	5,0	0,70
27	6,4	0,81	5,8	0,76	5,3	0,72	4,7	0,67	4,5	0,65
28	7,0	0,84	6,5	0,81	5,8	0,76	5,0	0,70	5,0	0,70
29	13,5	1,13	11,5	1,06	10,5	1,02	7,0	0,84	8,0	0,90
30	14,6	1,16	14,0	1,15	13,0	1,11	11,5	1,06	13,5	1,13
31	18,5	1,27	16,0	1,20	14,0	1,15	11,0	1,04	12,0	1,08
32									10,5	1,02
33	9,0	0,95	8,0	0,90	7,0	0,84	6,0	0,78	6,0	0,78
34	10,0	1,00	9,5	0,98	8,0	0,90	7,5	0,88	6,0	0,78
35	15,5	1,19	17,0	1,23	14,0	1,15	11,0	1,04	11,5	1,06
36									5,5	0,74
37							5,5	0,74	6,0	0,78
										0,74
38	7,8	0,89	7,5	0,88	6,0	0,78	5,5	0,74	5,5	

1	2	3	4	5	6	7	8	9	10	11
39									6,0	0,78
40	8,5	0,93	8,0	0,90	7,3	0,86	6,0	0,78		
41	14,0	1,15	13,0	1,11	12,5	1,10	10,0	1,00	10,5	1,02
42									8,0	0,90
43									8,5	0,93
44									8,5	0,93
45									8,0	0,90
46	8,0	0,90	7,5	0,88	6,5	0,81	6,0	0,78	7,0	0,84
47	9,0	0,95	9,0	0,95	7,5	0,88	6,5	0,81	6,5	0,81
48	10,5	1,02	9,5	0,98	8,0	0,90	7,5	0,88	9,0	0,95
49	9,3	0,97	9,0	0,95	7,5	0,88	6,7	0,83	7,0	0,84
50	13,0	1,11	13,0	1,11	10,5	1,02	9,5	0,98	10,5	1,02
51	12,5	1,10	12,5	1,10	10,0	1,00	8,5	0,93	10,0	1,00
52	9,0	0,95	9,0	0,95	8,0	0,90	6,5	0,81	7,0	0,84
53									6,5	0,81
54	14,7	1,17	14,0	1,15	12,0	1,08	10,5	1,02	13,0	1,11
55	10,5	1,02	11,0	1,04	9,0	0,95	7,5	0,88	9,0	0,95
56	7,0	0,84	7,0	0,84	6,0	0,78	5,0	0,70	5,0	0,69
57	10,5	1,02	10,0	1,00	9,5	0,98	7,7	0,89	10,0	1,00
58	11,0	1,04	10,0	1,00	9,5	0,98	7,0	0,84	8,5	0,93
59	16,0	1,20	15,0	1,18	13,0	1,11	11,0	1,04		
60	5,5	0,74	5,3	0,72	4,5	0,65	3,8	0,58		
61	20,0	1,30	19,0	1,28	17,5	1,24	12,8	1,11		
62	16,0	1,20	15,0	1,18	13,0	1,11	10,5	1,02	12,5	1,10
63	11,0	1,04	10,0	1,00	8,5	0,93	6,7	0,83		
64	15,0	1,18	14,5	1,15	12,5	1,10	10,0	1,00	10,0	1,00
65	8,0	0,90	7,5	0,88	6,0	0,78	6,0	0,78	6,0	0,78
66							7,0	0,84	9,0	0,95
67							12,5	1,10	15,0	1,18
68							12,0	1,08	12,0	1,08
69			15,3	1,18	12,0	1,08	14,5	1,16	15,0	1,18
70	10,0	1,00	9,5	0,98	7,0	0,84	6,7	0,83	7,0	0,84
71	9,5	0,98	8,5	0,93	8,0	0,90	7,2	0,86	8,5	0,93
72	16,5	1,22	15,0	1,18	14,0	1,15	11,5	1,06	12,0	1,08
73	13,5	1,15	13,0	1,11	11,0	1,04	9,0	0,95	9,5	0,98
74									13,5	1,13
75			17,0	1,23			12,2	1,09	13,5	1,13
76	11,0	1,04	10,0	1,00	9,0	0,95	8,0	0,90	8,5	0,93
77			13,3	1,12			10,7	1,03	11,5	1,06
78			11,0	1,04			8,0	0,90	9,0	0,95
79			9,0	0,95			7,2	0,86	7,5	0,88
80	17,0	1,23	15,0	1,18	13,0	1,11	11,0	1,04	12,0	1,08
81									11,5	1,06
82			14,0	1,15	11,8	1,07	10,2	1,01	12,5	1,10

1	2	3	4	5	6	7	8	9	10	11
83			8,7	0,90	6,8	0,83	5,8	0,76		
84	10,0	1,00	8,5	0,93	7,0	0,86	6,8	0,83	6,8	0,83
85	20,7	1,32	19,5	1,29	16,0	1,20	13,7	1,14	14,0	1,15
86	10,0	1,00	8,5	0,93	8,0	0,90	7,0	0,84	6,5	0,81
87	23,0	1,36	22,0	1,34	18,5	1,27	16,0	1,20	16,0	1,20
88			8,5	0,93	7,7	0,89	6,5	0,81	7,5	0,88
89			8,0	0,90						
90	21,0	1,32	18,5	1,27	14,5	1,16	12,8	1,11		
91	24,0	1,38	28,5	1,35	18,0	1,25	17,0	1,23	18,0	1,25
92	6,5	0,85	5,8	0,76	4,6	0,66	4,0	0,60	4,2	0,62
93	15,0	1,18	14,0	1,15	11,5	1,06	10,5	1,02	10,0	1,00
94	12,0	1,08	10,5	1,02	9,5	0,98	8,5	0,93	9,5	0,98
95	7,3	0,86	7,0	0,84	5,8	0,76	5,8	0,76		
96	21,0	1,32	20,0	1,30	17,0	1,23	14,5	1,16	14,0	1,15
97	21,0	1,32	20,0	1,30	17,0	1,23	14,2	1,15	14,5	1,16
98	20,0	1,30	19,0	1,28	16,0	1,20	14,0	1,15	14,5	1,16
99	16,0	1,20	15,0	1,18	12,0	1,08	9,2	0,96	10,0	1,00
100	13,5	1,13	13,5	1,13	12,0	1,08	11,0	1,04		

CATALOG KVARATSKHELIA

The minimum values of the degree of polarization (Pmin)

	Pmin (Int)	Pmin (4480Å)	lgPmin	Pmin (6400Å)	lgPmin
1	2	3	4	5	6
1	1,07	1,04	0,03	1,20	0,08
2	1,17	1,20	0,08	1,21	0,08
3	1,08	1,08	0,03	1,08	0,03
4	1,07	1,07	0,03	1,07	0,03
5	1,21	1,27	0,10	1,22	0,09
6	1,25	1,11	0,04	1,37	0,14
7	0,93	0,93	-0,03	0,93	-0,03
8	1,14	1,04	0,02	1,04	0,02
9	1,13	1,10	0,04	1,10	0,04
10	1,16	1,20	0,08	1,20	0,08
11	1,11	1,10	0,04	1,10	0,04
12	1,24	1,10	0,04	1,20	0,08
13	1,12	1,10	0,04	1,25	0,10
14	1,00	1,00	0,00	1,00	0,00

1	2	3	4	5	6
15	0,62	0,80	-0,10	0,70	-0,15
16	1,00	1,00	0,00	6,00	0,00
17	1,05	1,10	0,04	1,10	0,04
18	1,05	1,10	0,04	1,10	0,04
19	1,05	10,00	0,00	1,00	0,00
20	1,22	1,20	0,08	1,30	0,11
21	1,19	12,00	0,08	1,20	0,08
22	1,17	1,15	0,06	1,27	0,10
23	1,14	1,15	0,06	1,27	0,10
24	1,09	1,15	0,06	1,13	0,05
25	1,09	1,13	0,05	1,25	0,10
26	0,82	0,91	-0,04	0,98	-0,01
27	0,95	0,95	-0,02	0,95	-0,02
28	1,01	1,00	0,00	1,00	0,00
29	1,05	0,95	-0,02	0,95	-0,02
30	1,20	1,12	0,05	1,29	0,11
31	1,10	1,12	0,05	1,23	0,09
32	1,11	1,10	0,04	1,10	0,04
33	1,16	1,10	0,04	1,18	0,07
34	1,15	1,15	0,06	1,23	0,09
35	1,12	1,18	0,07	1,25	0,10
36	1,10	1,00	0,00	1,00	0,00
37	1,01	1,00	0,00	1,00	0,00
38	1,16	1,19	0,08	1,19	0,08
39	1,10	1,10	0,04	1,10	0,04
40	1,20	1,23	0,09	1,26	0,10
41		1,16	0,06	1,15	0,06
42	1,16	1,16	0,06	1,25	0,10
43	1,20	1,07	0,03	1,07	0,03
44	1,11	1,20	0,08	1,20	0,08
45	1,13	1,13	0,05	1,10	0,04
46	1,10	1,20	0,08	1,20	0,08
47	1,16	1,20	0,08	1,20	0,08
48	1,17	1,19	0,08	1,25	0,10
49	1,11	1,10	0,04	1,17	0,07
50	1,20	1,12	0,05	1,17	0,07
51	1,30	1,20	0,08	1,25	0,10
52	1,00	1,00	0,00	1,00	0,00
53	1,05	1,10	0,04	1,10	0,04
54	1,16	1,16	0,06	1,33	0,12
55	1,00	1,00	0,00	1,00	0,00
56	0,60	0,75	-0,12	0,67	-0,17
57	1,30	1,20	0,08	1,20	0,08
58	1,18	1,18	0,07	1,20	0,08

1	2	3	4	5	6
59	0,94	0,94	-0,03	1,10	0,04
60	1,01	1,00	0,00	1,00	0,00
61	1,07	1,04	0,02	1,12	0,05
62	1,27	1,25	0,10	1,20	0,08
63	1,07	1,07	0,03	1,07	0,03
64	1,10	1,14	0,06	1,13	0,05
65	0,74	0,72	-0,14	0,83	-0,08
66	1,05	1,05	0,02	1,00	0,00
67	1,15	1,15	0,06	1,20	0,08
68	1,20	1,20	0,08	1,20	0,08
69	1,10	1,22	0,09	1,25	0,10
70	1,13	1,16	0,06	1,10	0,04
71	1,21	1,21	0,08	1,20	0,08
72	1,05	1,10	0,04	1,12	0,05
73	1,11	1,11	0,04	1,20	0,08
74	1,21	1,21	0,08	1,25	0,10
75	1,20	1,23	0,09	1,25	0,10
76	1,12	1,12	0,05	1,10	0,04
77	1,30	1,30	0,11	1,30	0,11
78	1,21	1,21	0,08	1,20	0,08
79	1,12	1,12	0,05	1,10	0,04
80	1,25	1,15	0,06	1,30	0,11
81	1,30	1,30	0,11	1,30	0,11
82	1,31	1,01	0,00	1,20	0,08
83	1,15	1,10	0,04	1,10	0,04
84	0,85	0,99	0,00	0,97	-0,01
85	1,11	1,08	0,03	1,16	0,06
86	1,12	0,85	-0,07	0,84	-0,08
87	1,19	1,19	0,08	1,25	0,10
88	1,23	1,13	0,05	1,20	0,08
89	1,16	1,10	0,04	1,10	0,04
90	1,07	1,07	0,03	1,10	0,04
91	1,11	1,15	0,06	1,09	0,04
92	0,66	0,72	-0,14	0,69	-0,16
93	1,14	1,03	0,01	0,97	-0,01
94	1,05	1,05	0,02	1,10	0,04
95	1,09	1,09	0,04	1,10	0,04
96	1,19	1,10	0,04	1,25	0,10
97	1,20	1,20	0,08	1,25	0,10
98	1,03	0,97	-0,01	1,06	0,02
99	1,23	1,08	0,03	1,28	0,11
100	1,30	1,11	0,04	1,20	0,08

Albedo values for objects from the Catalog Kvaratskhelia Table 2

N	ρ**[3]** 4500Å	lgρ**[3]**	**ρ[4]** 4500Å	lgρ**[4]**	ρ**[5]** 5500Å	lgρ**[5]**	ρ**[6]** 5500Å	lgρ**[6]**	ρ**[7]** 6300Å	lgρ**[7]**
1	4	5	2	3	11	6	7	8	9	10
1	9,0	0,95	10,8	1,03	9,0	0,95	8,7	0,94	6,60	0,82
2	7,0	0,84	11,0	1,04	9,0	0,95	8,8	0,94	7,16	0,85
3	13,0	1,11	14,8	1,17	13,5	1,13	16,7	1,22	10,23	1,01
4	7,0	0,84	7,1	0,85	9,3	0,97	9,2	0,97	7,08	0,85
5	11,0	1,04	14,0	1,15	12,7	1,10	13,6	1,13	10,71	1,03
6	7,0	0,84	7,0	0,85	8,7	0,94	8,1	0,90	5,89	0,77
7	13,0	1,11	15,7	1,20	13,7	1,14	11,9	1,07	9,44	0,98
8	12,5	1,10	15,0	1,18	13,7	1,14	12,3	1,09	12,30	1,09
9	7,0	0,84	7,7	0,89	10,8	1,03	9,6	0,98	8,71	0,94
10	7,9	0,90	7,9	0,90	9,9	1,00	9,6	0,98	7,67	0,88
11	7,8	0,89	8,0	0,90	9,6	0,98	9,8	1,00	8,91	0,95
12	8,0	0,90	7,8	0,89	11,6	1,06	10,0	1,00	8,51	0,93
13	7,0	0,84	7,1	0,85	9,2	0,96	9,0	0,95	7,08	0,85
14	7,1	0,85	7,1	0,85	9,6	0,98	9,6	0,98	9,33	0,97
15	17,0	1,23	14,5	1,16	18,6	1,27	21,0	1,38	16,22	1,21
16	7,3	0,86	7,1	0,85	9,5	0,98	9,6	0,98	9,33	0,97
17	15,5	1,19	14,2	1,15	16,4	1,21	14,3	1,15	11,75	1,07
18	13,0	1,11	12,0	1,08	13,0	1,11	13,1	1,12	11,09	1,04
19	8,0	0,90	8,0	0,90	10,2	1,01	12,2	1,09	11,09	1,04
20	8,0	0,90	8,0	0,90	10,5	1,02	10,1	1,00	8,51	0,93
21	9,0	0,95	11,5	1,06	11,4	1,06	11,5	1,06	9,44	0,97
22	7,0	0,84	7,0	0,84	8,5	0,93	7,7	0,89	5,96	0,78
23	9,0	0,95	8,6	0,93	11,4	1,06	11,5	1,06	8,91	0,95
24	12,0	1,08	9,5	0,98	12,7	1,10	13,0	1,11	10,72	1,03
25	8,1	0,91	9,0	0,95	10,8	1,03	10,6	1,02	9,12	0,96
26	16,0	1,20	13,5	1,13	14,6	1,16	17,9	1,85	15,85	1,20
27	16,0	1,20	14,0	1,15	15,6	1,19	19,6	1,29	17,78	1,25
28	15,0	1,18	14,0	1,15	16,0	1,20	16,7	1,22	13,80	1,14
29	8,5	0,93	7,0	0,84	10,6	1,02	13,1	1,11	10,59	1,02
30	7,0	0,84	7,0	0,84	9,4	0,97	8,2	0,91	7,00	0,84
31	7,0	0,84	7,0	0,84	9,9	1,00	9,4	0,97	7,85	0,90
32	7,3	0,86	7,0	0,84	10,2	1,01	10,1	1,00	8,91	0,95
33	11,0	1,04	10,3	1,01	13,7	1,14	17,5	1,24	11,22	1,05
34	12,5	1,10	11,0	1,04	12,0	1,08	12,6	1,10	9,88	1,00
35	7,0	0,84	7,5	0,88	9,8	0,99	9,2	0,97	7,50	0,88
36	13,0	1,11	12,0	1,08	14,6	1,16	15,1	1,18	11,61	1,06
37	9,5	0,98	7,9	0,90	16,9	1,23	16,0	1,20	13,96	1,14
38	13,5	1,13	14,0	1,15	15,1	1,18	15,1	1,18	11,88	1,07
39	12,0	1,08	7,2	0,86	14,2	1,15	15,1	1,18	11,75	1,07

1	4	5	2	3	11	6	7	8	9	10
40	13,0	1,11	11,0	1,04	13,8	1,14	14,3	1,15	11,09	1,04
41	8,5	0,93	9,0	0,95	10,8	1,03	8,9	0,94	10,47	1,02
42	9,0	0,95	9,0	0,95	11,5	1,06	11,8	1,07	9,77	0,99
43	9,5	0,98	9,0	0,95	12,2	1,09	12,1	1,08	9,66	0,98
44	10,0	1,00	8,0	0,90	7,7	1,10	12,1	1,08	9,88	0,99
45	8,5	0,93	8,1	0,91	10,5	1,02	12,4	1,08	11,09	1,04
46	12,9	1,11	12,0	1,08	14,6	1,16	15,5	1,19	12,30	1,09
47	12,0	1,08	12,1	1,08	13,0	1,11	12,9	1,11	11,09	1,04
48	10,0	1,00	12,0	1,08	12,8	1,11	12,9	1,11	10,00	1,00
49	10,0	1,00	11,8	1,07	13,4	1,13	13,3	1,12	11,09	1,04
50	7,3	0,86	8,0	0,90	10,8	1,03	10,3	1,01	8,61	0,93
51	8,0	0,90	13,0	1,11	10,3	1,02	10,5	1,02	8,71	0,94
52	11,0	1,04	12,0	1,08	12,9	1,11	12,9	1,11	11,35	1,05
53	8,0	0,90	11,0	1,04	11,4	1,06	12,3	1,08	12,59	1,10
54	11,0	1,04	12,0	1,08	9,3	0,97	9,3	0,97	7,16	0,85
55	9,0	0,95	7,7	0,89	11,4	1,06	10,0	1,00	10,59	1,02
56	18,0	1,25	16,0	1,20	16,2	1,21	19,3	1,28	16,03	1,20
57	9,0	0,95	7,5	0,88	11,6	1,06	12,8	1,11	9,66	0,98
58	8,0	0,90	8,5	0,93	10,8	1,03	10,7	1,02	9,12	0,96
59	7,0	0,84	7,0	0,84	9,0	0,95	8,5	0,92	6,61	0,82
60	16,0	1,20	17,0	1,23	16,0	1,20	17,8	1,25	13,96	1,14
61	7,1	0,85	7,1	0,85	9,3	0,97	9,3	0,97	7,50	0,88
62	7,0	0,84	7,4	0,87	9,5	0,98	9,4	0,97	6,76	0,83
63	8,9	0,95	7,9	0,90	12,0	1,08	12,4	1,10	9,77	0,99
64	9,0	0,95	7,5	0,88	12,0	1,08	12,4	1,10	9,44	0,98
65	15,0	1,18	12,4	1,09	15,5	1,19	17,3	1,23	12,88	1,11
66	7,5	0,88	7,6	0,88	10,8	1,03	13,1	1,12	11,35	1,05
67	7,0	0,84	7,3	0,86	8,5	0,93	9,5	0,89	7,58	0,88
68	7,0	0,84	7,0	0,84	9,4	0,97	9,9	1,00	8,51	0,93
69	7,0	0,84	7,0	0,84	8,5	0,93	8,2	0,95	6,31	0,80
70	11,0	1,04	7,0	0,84	11,4	1,06	14,0	1,15	13,18	1,12
71	10,0	1,00	9,3	0,97	11,7	1,07	11,0	1,04	10,23	1,01
72	7,0	0,84	7,5	0,88	9,5	0,98	9,6	0,98	7,08	0,85
73	8,0	0,90	7,9	0,90	10,8	1,03	10,7	1,02	7,67	0,88
74	7,5	0,88	7,7	0,89	9,6	0,98	9,5	0,98	7,08	0,85
75	10,2	1,01	7,2	0,86	9,5	0,98	9,7	0,98	7,08	0,85
76	7,9	0,90	7,5	0,88	11,1	1,04	12,8	1,11	9,84	0,99
77	7,4	0,87	7,5	0,88	9,5	0,98	8,9	0,94	7,58	0,88
78	7,8	0,89	7,1	0,85	11,4	1,06	13,2	1,12	7,00	0,84
79	9,0	0,95	9,0	0,95	12,0	1,08	15,3	1,18	10,12	1,00
80	7,1	0,85	7,0	0,84	9,1	0,96	9,3	0,97	7,67	0,88
81	7,4	0,87	7,4	0,87	9,2	0,96	9,7	0,98	10,47	1,02
82	7,0	0,84	7,2	0,86	9,5	0,98	11,5	1,06	7,58	0,88
83	12,0	1,08	12,0	1,08	12,7	1,10	14,5	1,16	10,59	1,02

1	4	5	2	3	11	6	7	8	9	10
84	10,8	1,03	11,0	1,04	12,8	1,11	16,6	1,22	11,75	1,07
85	6,8	0,83	7,0	0,84	8,0	0,90	8,2	0,98	6,53	0,81
86	9,0	0,95	8,0	0,90	11,4	1,06	14,4	1,15	11,61	1,06
87	6,0	0,78	7,0	0,84	7,8	0,89	7,7	0,88	5,82	0,76
88	10,5	1,02	10,5	1,02	11,4	1,06	12,6	1,10	6,46	0,81
89	11,0	1,04	9,5	0,98	11,4	1,06	14,6	1,16	8,32	0,92
90	6,1	0,78	6,5	0,81	7,9	0,90	10,4	1,02	8,81	0,94
91	6,0	0,78	6,5	0,81	7,6	0,88	7,4	0,87	5,43	0,73
92	12,0	1,34	10,0	1,00	12,7	1,10	20,4	1,31	17,78	1,25
93	8,0	0,90	8,0	0,90	9,5	0,98	10,9	1,04	8,41	0,92
94	9,0	0,95	9,5	0,98	12,7	1,10	11,9	1,07	12,30	1,09
95	13,0	1,11	12,7	1,10	13,4	1,13	18,3	1,26	10,59	1,02
96	6,3	0,80	6,4	0,81	8,1	0,91	9,6	0,97	6,46	0,81
97	6,6	0,82	6,7	0,83	7,9	0,90	9,4	0,97	6,31	0,80
98	6,3	0,80	7,0	0,84	7,9	0,90	10,0	1,00	7,24	0,86
99	7,0	0,84	8,2	0,91	7,4	0,87	12,9	1,11	8,91	0,95
100	6,7	0,83	8,9	0,95	8,9	0,95	8,8	0,98	6,53	0,81